Bachelor Thesis

Sander Kamerbeek

June 2008 - December 2008

Fabrication of a planar optical waveguide cleaved with micrometer precision

University of Groningen
Faculty of Mathematics and Natural Sciences
Department of Applied Physics
Research group: Physics of Nanodevices
Group leader: Prof. dr. ir. B.J. van Wees
Supervisor: Dr. Ir. C.H. van der Wal
Supervisor: Ir. M. Sladkov

Abstract

For the research involved with the realization of a optical memory element it is necessary to fabricate waveguides. The wafer used to create these waveguides has a heterostructure top layer which forms the waveguide. Etching the top layer of the wafer allows for determining the dimensions of the waveguide. The challenge is to fabricate a waveguide which is as close as 1 μm from the wafer edge. To meet this challenge a method is developed for cleaving off excess substrate material with a precision in the order of micrometers. After introducing a double scribe in the GaAs wafer it is possible to predict the wafer cleaving location with a precision of a micrometer. The edge of the cleaved wafer shows sub micrometer roughness and therefore allows the placing of a waveguide entrance as close a 1 μm from the wafer edge. There is however a small chance the sample will not be break smooth enough at the predicted location. This could result in destroying the final device since cleaving is the last step in the fabrication process. Etching channels in a wafer, mimicking a scribe, does not result in pinning down the location the wafer breaks when cleaved. An attempt was made to fabricate waveguides using gold as an etching mask. This failed, most likely because the adhesion metal, titanium, between the GaAs sample and the gold is dissolved in the etching mixture of H_2SO_4:H_2O_2:H_2O.

Some basic equations for a symmetric planar waveguide where derived giving insight in the basic workings of the device. The coupling efficiency of the waveguide input was calculated to be 0.3702 taking into account Fresnel reflection at the end face of the waveguide at normal incidence. The waveguide is shown to be single mode and has a NA of 0.58.

Contents

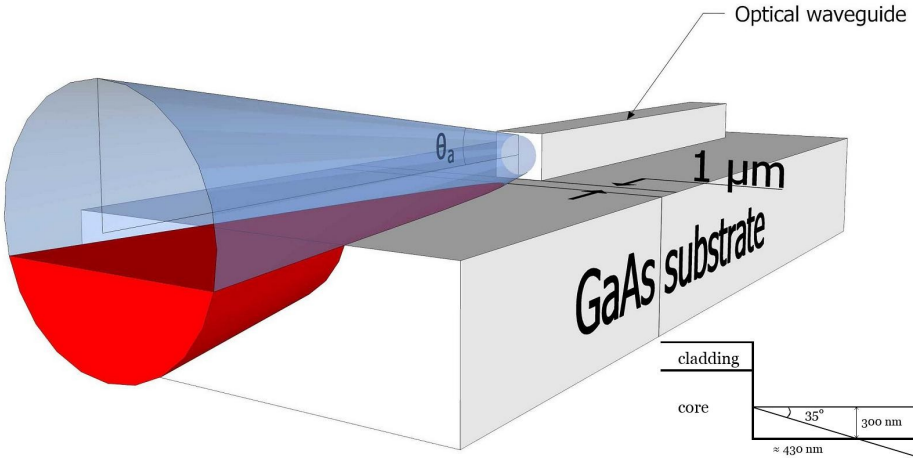

Figure 1: The red part of the cone of light is blocked due to the GaAs substrate. If the substrate is cleaved at the position indicated by the line on the side of the substrate the full cone of light is able to enter the waveguide. The acceptance angle is half the angle of the cone and denoted with θ_a. In the left bottom the cleave distance is calculated to be approximately 430 nm.

1 Introduction

A big challenge in physics is to realize practical quantum information technology. Research is proposed by Maksym Sladkov, a PhD from the same group, which aims at building a memory element for optical pulses, that can preserve the quantum state of the optical pulse. Such a memory element is crucial to make long distance optical quantum communication possible. For this research it is necessary to couple laser light into a waveguide. The aim of this research project is to fabricate a waveguide in such a manner that all laser light can be coupled into the waveguide.

A waveguide consists of a core of dielectric material which is surrounded by another dielectric material called the cladding. The refractive index of the core is slightly higher than that of the cladding thus making total internal reflection (TIR) possible. Due to TIR it is possible to guide electromagnetic waves with negligible loss and preservation of their transverse spatial distribution. TIR inside the waveguide occurs only for light coupled into the waveguide with an angle smaller then the acceptance angle θ_a. This angle is expressed by the numerical aperture NA[1] of the wave guide.

The waveguide used in this research project consists of Aluminum Gallium Arsenide (AlGaAs). Light is focused on the end-face of the waveguide with a lens to couple in light. The waveguide used in this project has an NA of approximately 0.58. To obtain the highest possible optical power inside the waveguide it is paramount to couple in light over the full range of the acceptance angle of 35 °. The fabrication method of the waveguide does not permit such a cone of light to be coupled into the waveguide because the waveguide lies on top of a GaAs substrate. The surrounding substrate material blocks the lower half of the accepted cone of light (figure 1).

The first goal of this project is to create a waveguide which can accept a cone of light with a numerical aperture of approximately 0.58. To couple in light in the waveguide in the full range of the acceptance angle the entrance has to be fabricated approximately 0,5 µm away from the GaAs substrate edge (left bottom of figure 1). The most precise way to cleave a wafer is by using a scribe made by a diamond tip. The minimum width of the scribe is on the order of 2 to 3 µm, it is therefore possible but close to the limitations of

[1] $NA = \sin(\theta_a) = \sqrt{n_1^2 - n_2^2}$; where n_1 and n_2 are refractive indices of the core and cladding respectively.

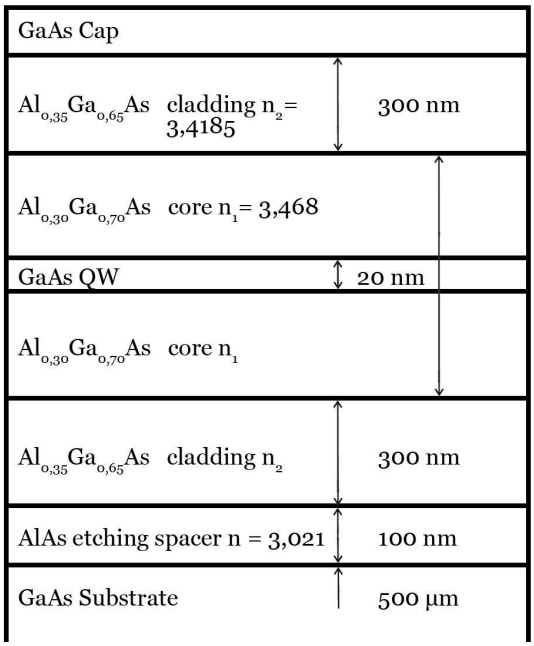

Figure 2: The structure of the epitaxially grown top layer on top of the 500 µm thick GaAs substrate

this technique to cleave with such precision.

The second goal of this report is to characterize the coupling of the light with and the propagation of light in the waveguide. Since the light ray is actually a propagation of an transverse-electromagnetic (TEM) wave the modes inside the waveguide are a solution of the wave equation. The width of the waveguide as well as the refractive indices and the wavelength of the incident light determine how many modes can be sustained by the waveguide. These modes will propagate through the dielectric medium with different velocities and different amplitudes. Of special interest is the possibility of mode-coupling. This is the transition of the TEM-wave inside the medium from being completely determined by the lowest mode and its decay to other modes when the wave transverses the waveguide due to non-linear optical effects.

2 Creating a free accessible waveguide entrance

2.1 Waveguide manufacture and limitations

The wafers are prepared by the group of Dr. D. Reuter & Prof. A.D. Wieck in Bochum and have a special grown waveguide layer on top. The bulk of the wafer is a normally grown 500 µm thick layer of GaAs. This Layer of GaAs serves as a substrate on which the different layers which form the waveguide are grown. This top layer is a epitaxially grown layer and is very thin compared to the GaAs bulk (figure 2). The waveguide itself is composed of three different compounds. In the middle is a GaAs quantum well (QW). This QW is sandwiched in between a layer of AlGaAs which itself is in between a different layer of AlGaAs. The two layers of AlGaAs differ in their composition. The ratio of aluminum to gallium contents results in a difference in refractive index thereby creating a waveguide.

The shape of the desired waveguide can now be created by etching out a pattern in the top layer of the wafer. A photoresist, which is spun on the wafer, can be used to serve as an etch mask. Electron beam lithography (EBL) can be used to transfer the desired waveguide pattern in the resist.

To create patterns in a photoresist with EBL is an easy to use technique which can achieve nanometer precise resolution. It is, however, virtually impossible to use this techniques on the edge of a sample because the layer of photoresist will vary greatly in thickness near the edge, or might not cover the sample at all. This is because the layer of photoresist is coated on the sample with the use of a spindler which only gives a uniform layer of resist in the center of the sample. It is therefore impossible to create the waveguide structure on the edge of the sample.

Consequently the waveguide has to be manufactured in the center of the wafer. When the waveguide pattern is etched out of the wafer it is surrounded by GaAs bulk material. The material in front of the waveguide entrance restricts the angle at which the laser light can be shone in the waveguide. This effectively reduces the intensity with which the waveguide can be illuminated. To overcome this problem the material in front of the waveguide entrance has to be removed up to 0.5 μm from the waveguide to obtain a free accessible waveguide entrance.

2.2 Methods for creating a free accessible waveguide entrance

During the project several methods to solve the blocking of the light by the GaAs bulk material where investigated. All methods will be discussed and their usefulness evaluated.

2.2.1 Wafer cleaving process

It is a very common practice to cleave a crystalline wafer in smaller pieces by introducing a cut in the sample. There are numerous ways to create such a cut. An easy to use technique is to use a diamond tip to scribe a cut on the surface of the crystalline wafer with the help of a Scriber.

The device used to make the scribe on the sample, which will be referred to as the Scriber, is very basic. The sample is mounted on a plateau which can be moved and rotated. Under the sample is a small cavity where a pump creates a vacuum thereby holding the sample in its place. Above the plateau is the arm in which the diamond tip which will make the scribe is mounted. The plateau is inspected through a microscope. The sample is positioned in such a way that the scribe will be made as close to a {100} direction of the wafer as possible. When looking through the microscope there is a cross which can be used to align the wafer with respect to the diamond tip. This cross can then be used to position the scribe, however, the scribe location and the cross indicator are not aligned correctly with a scribe being made approximately 30 μm to the right of the cross when viewed through the ocular. The depth of the scribe can be varied by making several scribes, which increases the depth and width, or by slightly lifting the arm, decreasing the depth and width. The Scriber also has a measurement tool which is accurate up to 0,1 micrometer to characterize the dimensions of the sample.

To break the wafer along the cut that was scribed a simple cleaving device can be used to which will be referred as the Cleaver.

The sample is covered between two sheets of transparent thin flexible plastic. It is then placed between a movable transparent holder and the bottom plate of the Cleaver with the scribed line just over the edge of the bottom plate. The lever is then positioned so it will hit the outermost edge of the sample. The transparent holder will be pressed down and so locking the sample in it's location. Finally a small force will be applied quickly on the lever so it will hit the sample for a very brief moment. If the scribe was made correct the sample will break along the scribed line. At the location of the scribed line the sample will have a rough texture but where the crack propagates through the unscripted wafer it will ,ideally, be along one crystallographic plane and thus have a straight and smooth texture.

This technique could be used to cleave off the GaAs material in front of the waveguide entrance.

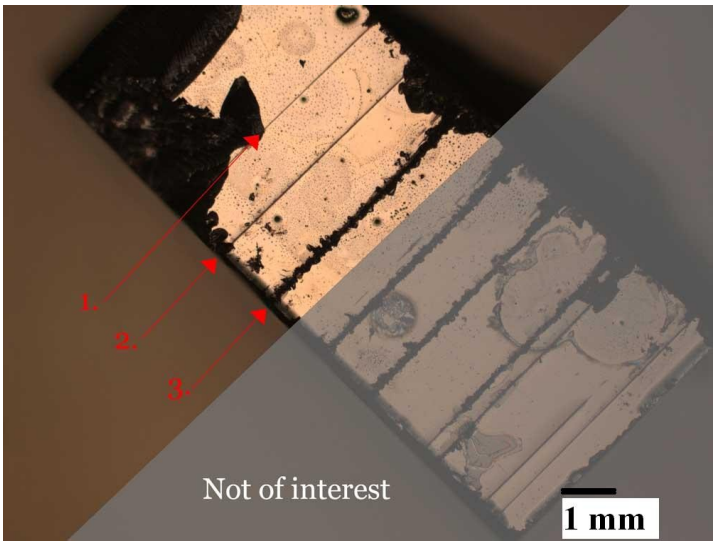

Figure 3: GaAs sample with several cuts varying in width and therefore depth. Scribe 1 is 2 µm deep and 5 µm wide, scribe 2 is 3 µm deep and 12 µm wide and scribe 3 is 4 µm deep and approximately 50 µm wide.

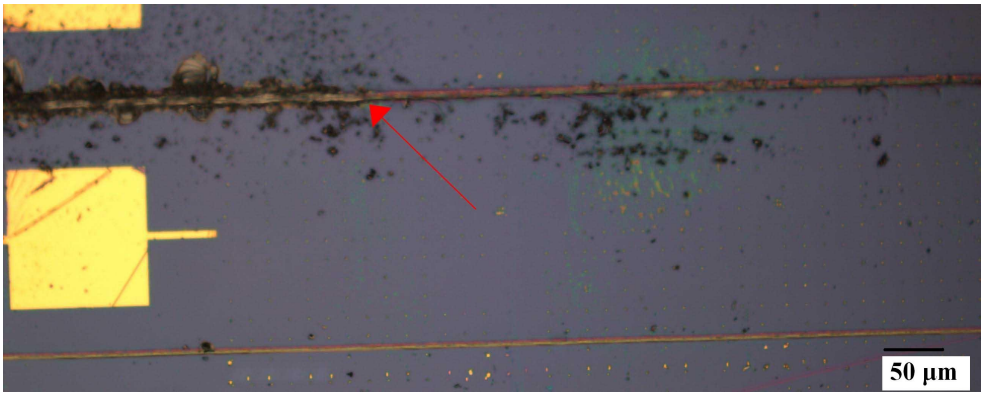

Figure 4: The upper left of the top cut shows a core which is colored lightly and has a consistent width. Surrounding this core are patches of damaged sample of which the width fluctuates. At the location indicated by the arrow the diamond tip was lifted slightly resulting in a less deep cut and less surrounding damage. The scribe in the bottom is the lightest scribe possible and shows almost no damage to the surrounding area. The width of this cut is approximately 5 µm. The sample is a piece of SiO_2/Si

There are a couple of condition which need to be satisfied when using this technique to use it successfully:

1. Cleaving the wafer should result in a crack propagation through the wafer which is highly predictable.
2. The edges of the cleaved part of the wafer should have a roughness well below a micrometer.
3. The scribe will be made prior to spinning the photoresist which could change the uniformity of the resist. The photoresist spun on the wafer must be uniform enough to be usable in the EBL machine.

2.2.2 Analysis of a diamond scribe

The first step was to determine the depth and width of a scribe. This was done with two different wafer types. The first wafer was a silicon p-doped wafer. This wafer was used

because it was readily available as junk material in the FND group. It was therefore suitable to use to get some experience in using the Scriber. For the final measurement a piece of Sumitomo wafer was used and the profiles of the scratches were analyzed with a DekTak. profile meter. The scribes differ in depth by varying the number of times the diamond tip scribed the same location (figure 3).

The first line on the upper left is so thin the DekTak cannot measure the width and depth. This line was created by scribing the sample once and also lifting the diamond tip slightly. The lifting results in a reduction of force with which the diamond tip is pressed on the sample resulting in a shallower scribe. The DekTak has a spatial resolution of 6.5 μm and so the width of this line has to be under 6.5 μm. Using AFM would resolve this problem however there was no time to become proficient with the AFM and could therefore not be used. It also proved difficult to determine the width and depth of the heaviest scribed lines because these scribes resulted in a lot of damage to the area surrounding the cut. A single scribe will look like the smooth scribes as the upper two left cuts in figure 3. When another scribe is made on the same location the cut gets deeper but the material directly surrounding the initial cut gets deformed. Chips are formed along side the scribe and debris is launched from the scratch and hits the surrounding wafer doing considerable damage to the wafer top layer as is seen by optical microscope inspection (figure 4).

When analyzing the sample with the DekTak it is difficult to distinguish these surrounding patches, i.e. the formation of chips at the sides of the scratch, from the core unless a lot of different scans are made. This would be too much effort for the relevance of the data and was therefore not investigated.

The maximum depth of a scribe is 4 μm and the maximum width is found to be 50 μm corresponding to scribe number 3 from figure 3. However with microscope inspection it is clearly visible that the width of the core, which is colored lightly, is maximally 15 to 20 μm. There is a positive correlation between the width and the depth of a scribe, however, the exact dependence is unknown. Since it is impossible to determine the depth of a scribes having a width of 12,5 μm or lower the width will be the dimension used in analyzing different scribes.

The next step was to analyze what the minimum depth and width of the scribe should be to be able to pin the cracking of the sample at the scribed location. Cleaving test were done on several samples, both Si and GaAs, with scribes in the full range of widths possible. All scribes resulted in breaking the wafer at the scribed location, therefore increasing the depth does not seem to have a noticeable influence on pinning the crack location of the wafer.

The deeper cleave lines result in a lot of debris production. When scribing the deeper lines some of the material which is scratched away is launched to the side and hits the wafer surrounding the scratch. This can result in very deep indentations and thus damage the top layer of the wafer. This effect can be seen in figure 4 where the indentations are the dark patches surrounding the upper cut. By making very thin scribes the amount of damage can be greatly reduced. If however the damage is caused by the side of the tip hitting the wafer, deeper scratches could be made without the extensive damage to the surrounding by using a tip with a smaller broadening angle (i.e. a longer and sharper point).

Figure 6: On the left: two scribes have been made in the wafer with a unscripted gap in between. On the right: only one scribe has been made. Note: the width and length of the scribes are not in proportion to the size of the wafer.

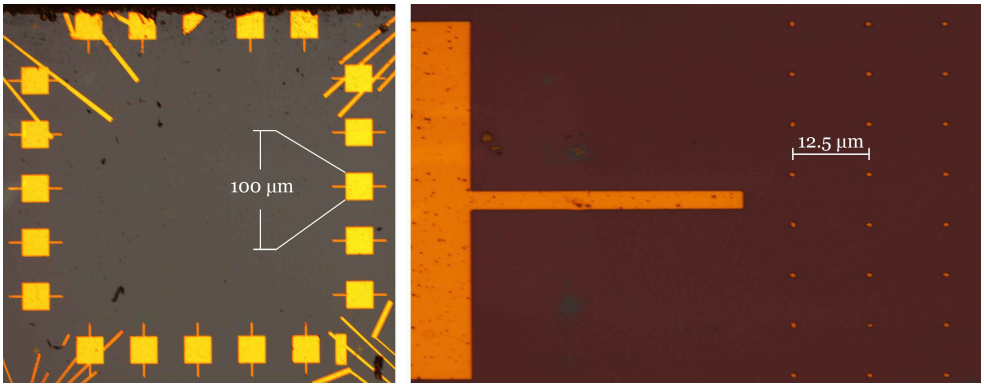

Figure 5: On the left: the grid of gold contact pads on the silicon sample. On the right: a gold contact pad with the grid of dots next to it. The spacing of the dots is 12,5 µm. The grids formed by these gold features is used to track the crack propagation when the sample is cleaved.

2.2.3 Cleaving a silicon wafer

Although the thinnest scribe causes less debris and has a smoother profile then the deeper scribes there is still too much deformation surrounding the scribe to manufacture waveguides 1 µm from the scribes. It is therefore necessary to make a scribe only partly over the sample which after cleaving would result in a crack which propagates through the unscripted wafer part. This can be done in two ways (figure 6).

The first method is to make two scribes leaving an unscripted spot between them where the crack will propagate from one scribe through the other. The other way would be to make one scribe and let the crack propagate from the scribe end towards the sample edge.

To determine the propagation of the crack through the wafer there need to be markers on the wafer which can be used as a reference. To make a wafer which has these markers would require the assistance of a group member which was a problem since the group was understaffed at the time. Therefore the wafers which are used are waste material from another research project in the FND group. These however are silicon wafers and the obtained results can therefore not be translated to GaAs wafers. However GaAs tends to break cleaner and smoother then silicon so the silicon should give a good indication for the possibility of this approach. Also there are plenty of silicon wafers but GaAs is very scares and was therefore not readily available. The sample is covered with 2 different grids. The first consists of contact pads which are 100 µm wide. The second grid consists of small dots which are spaced 12,5 µm apart (figure 5).

The contact pads were used to align the diamond scriber so a straight scribe perpendicular to the row of contact pads could be made. The grid of small dots had two uses. The first was to determine the precision with which the scribe can be placed on the sample. The second was to determine how the crack propagates through the sample when it is cleaved. With a spacing of 12,5 µm it is possible to follow the crack propagation with micrometer accuracy.

The double scripted wafers results in a crack propagation more collinear to the scribe then a single one. Possibly the second cut guides the propagation through the wafer towards itself. Based on optical observation it looks like a crack will always form at one of the cuts then propagating through the wafer towards the other side.

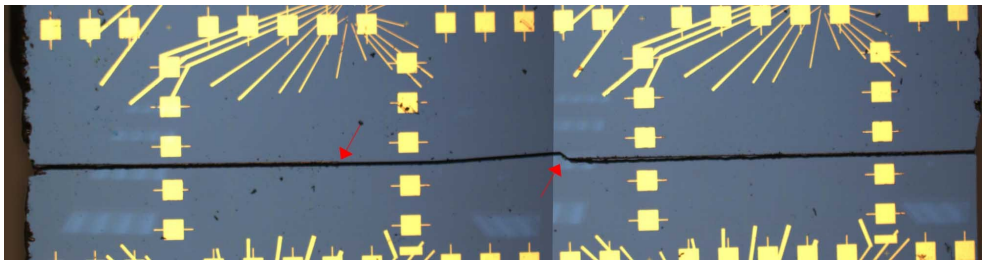

Figure 7: The crack was initiated at the left side of the wafer (left arrow) and then propagated towards the right. This can be seen because it smoothly curves from the initial breaking location and then abruptly breaks back to the other cut (right arrow). The two resulting pieces of wafer are placed together under the microscope as close as possible. The separation between them is the black band. All upcoming pictures of cleaved wafers are placed together in this manner.

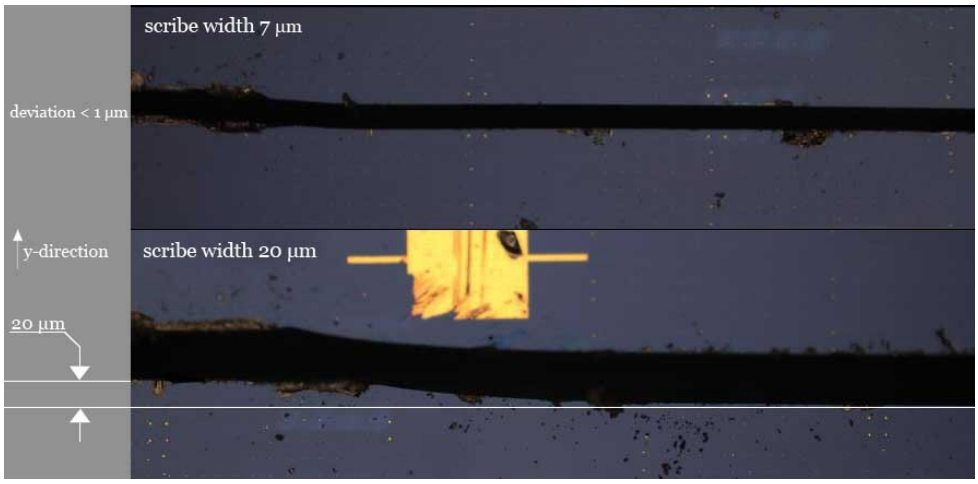

Figure 8: The width and thus depth of the scratch has profound influence of the amount of curving of the crack propagation. The deeper the cut the more the crack will curve. The upper cut has a width in the order of 7 µm, the lower cut has a width of 20 µm. The cuts are the origin of the crack location therefore the propagation direction is to the right.

A crack will always curve away from one of the scribes. Due to the curving when the crack reaches the second scribe it is not at the location of the second scribe. However the second scribe has such profound influence on the wafer that it forces the wafer to crack there and thereby forcing the crack to bend back to the second scribe (figure 7). It seems therefore plausible to assume that the initial cracking location is the location where the scribe smoothly starts to curve. The wafer will crack at the center of the scribe as is known from literature. The crack propagates very straight when close to the scribe initiating the crack. If the initial cracking location could be determined this would greatly improve the accuracy of this method.

The depth of the scribe has an important influence on the crack propagation through the unscripted part of the wafer. The deeper the scribe the more curved the crack propagation becomes (figure 8).

After this curve the crack would propagate almost perpendicular to the scribe made by the diamond tip. If the amount of displacement in the y-direction and the distance over which this crack propagates in the y-direction could be predicted it would be possible to manufacture the waveguides close to the crack. Unfortunately it appeared to be very difficult to correlate the amount of curving and the distance over which it curved to the depth and width of the scribe precisely.

However, the propagation of the crack of the thinnest scribe gave a deviation from the edge of the scribed line of 10 µm over a length of 1 mm. With such a precision it will not be necessary to take the curving into account. This precision will be good enough to make an educated guess where to manufacture the waveguides to be close enough to the

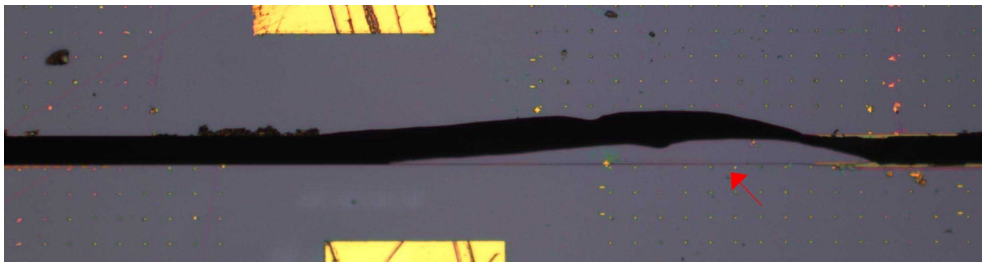

Figure 9: When the gap between the two cut becomes smaller than 500 µm the silicon wafer will crack at two location. One, very shallow crack, continuing the straight path (indicated by arrow), the second bending away.

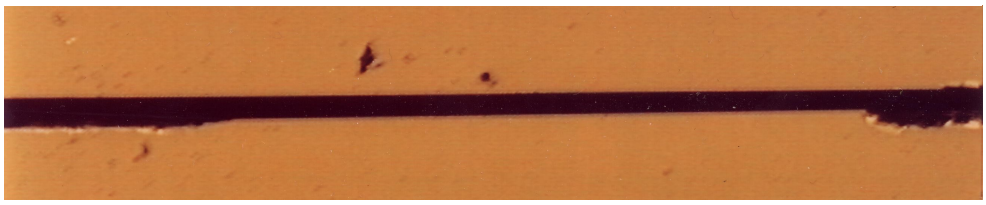

Figure 10: A cleaved GaAs wafer inspected under the microscope. The crack propagates without any visible curving and results in a much cleaner break than in a silicon wafer.

crack site.

Since the size of the waveguide will have a lateral width of approximately 1 µm there is no need for a gap between the two cuts exceeding the 200 µm. However, when there is a gap of less than 500 µm between the two cuts another effect comes into play. The crack will propagate towards the second cut with no curving. But when the crack has propagated half way a second crack will form. This second crack, which actually breaks the sample, will deviate from a straight path and bend away. Until it is close to the second cut and abruptly bends back. The second crack, which is much smaller, continues the straight path but does not result in actually breaking the wafer (figure 9). The reason for this phenomenon is unclear. Due to this problem the two cuts can not be too close to each other, further complicating the process.

2.2.4 Cleaving a GaAs wafer

The cleaving of a GaAs wafer with the double scripted scribe configuration proved to be much easier then the silicon wafer (figure 10). It breaks so much better than silicon that almost all the information obtained by the silicon wafers tests have no relevance for GaAs. There seems to be some correlation between the curving of the crack propagation and the depth of the scribe but it is much weaker than with silicon. Any bending of the crack propagation stays well below a deviation of several micrometers over a length of a millimeter. Another possible important factor in obtaining a straight crack line is the precision with which the scribe can be made parallel to a <110> crystallographic direction for (100) grown wafers. Since the pieces of GaAs used in the research where often already used by Maxim Sladkov it was difficult to align a scribe to a crystallographic axis. The edges of the samples often were not smooth enough to determine the direction of the crystallographic axis. The positioning of the scribe can also be greatly increased by using a microscope with higher magnification on the Scriber. With the current scribe setup it is not practical to make scribes closer to each other then approximately 200 µm.

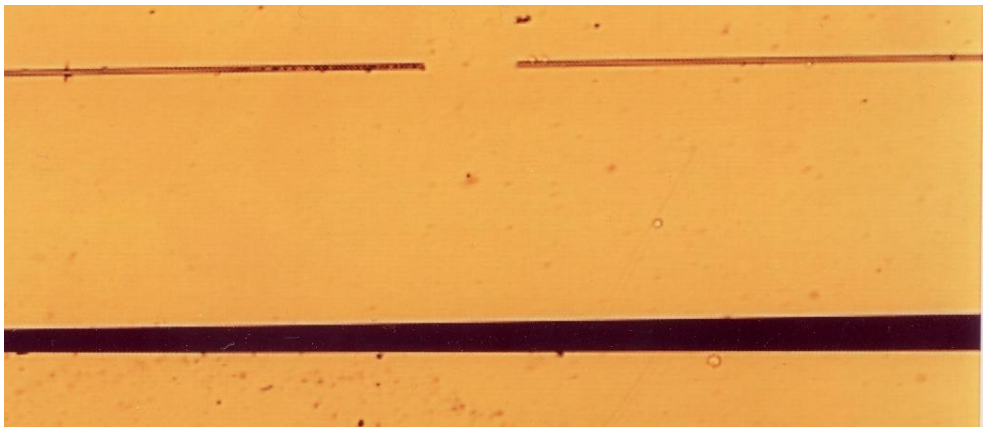

Figure 11: The upper stripes are the etched grooves and have a width of 2 μm. After cleaving the wafer broke however not at the location of the etched grooves.

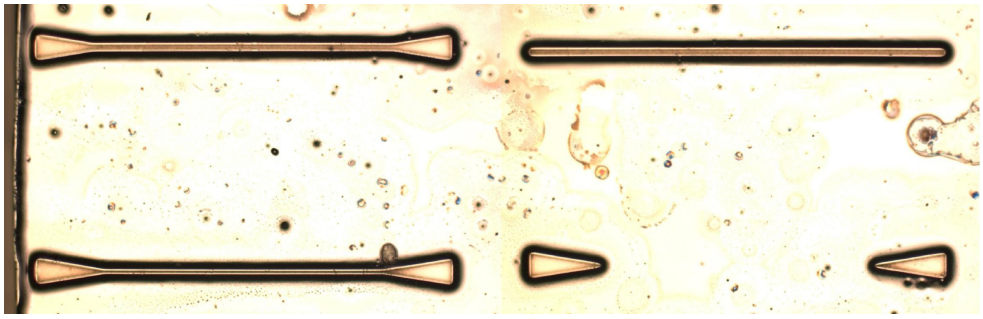

Figure 12: The 4 different geometries after etching. All grooves have a flat plateau in the middle which is 200 nm higher than the lowest point of the black edges of the grooves. See Appendix A.2 for fabrication details.

2.2.5 Cleaving the sample with an etched groove

The cleanroom of the FND group has three methods of etching available: wet etching, reactive ion etching (RIE) and sputter etching. Unfortunately wet etching is the only etching technique available in the cleanroom to etch the channel dimensions which are needed. The etching depth of sputtering techniques is limited to at most a couple of hundred nanometers due to the heating of the sample. For RIE chlorine gas is needed to etch through the AlGaAs, which is not possible because the chamber is made of aluminum and would therefore also be attacked during the etching process. RIE would be the etching process of choice since it is highly anisotropic, allowing the etching of very thin but deep channels. However, using RIE would also damage the quantum well in the waveguide thereby rendering RIE useless.

The disadvantage with the diamond scribe method is the lack of precision with which the scribe can be made. It also proved difficult to predict on which side of the scribe the crack would propagate. Another disadvantage is the low reproducibility of the process since not every scribe cracks without bending away from a straight path.

These problems could be overcome if the diamond scribe tool could be replaced by a process which makes a highly reproducible cut in the sample. One way of obtaining such high reproducibility is by etching channels in the sample. The channels would be completely characterized by the EBL pattern transfered in the photoresist on the sample, the etchant and its concentration used. Therefore the dimensions of the channels can be controlled very precisely. The question arises whether these etched channels will also result in forcing the wafer to crack at the channel location, like the scratch with a diamond tip does. Since the method of creating a cut in the sample by making a scribe or etching a channel rely on completely different physical processes. The diamond tip creates a cut by exerting a mechanical force on the sample and scratching the material from the bulk whereas the etch agent creates a channel by dissolving the wafer. A scratch introduces

extensive dislocations and other stresses in the wafer surrounding the location of the scribe. Wet etching only removes the material and introduces no or negligible stresses.

The first step was to redo an experiment done by FND-group member ir. Ji Liu who tried breaking a sample using the etching process. Although the attempt of ir. Ji Liu failed, redoing the process would possibly lead to some clues for a next step procedure. The geometry of the first sample was intended to imitate a scribed cut. The sample has a rectangular channel etched in the wafer parallel to the top of the sample, much like the upper right geometry in figure 12. The channel does not extend to the edges of the wafer due to the limitations of the resist spinning process discussed earlier. For a cut made by the diamond tip this small offset from the edge has no influence on pinning the crack location or propagation. The exact geometry as well as all fabrication procedures are in Appendix A.1. The width of the channel is 2 μm which is 3 to 5 μm smaller than the thinnest cut possible. The wafer, after etching, shows the desired channel. However some plateau is formed in the middle of the channel as was seen by DekTak profile meter inspection. The reason for the forming of this plateau is unknown. Since the width of the channel is too small to measure no DekTak reading can be done to determine the height of the plateau. New samples with a wider channel can be used to determine the plateau hight with the DekTak assuming the effect will also show. It might also be that the bottom of the channel reflects light much better then the curved side walls and therefore appears to be a plateau.

After cleaving the sample it broke in two separate parts. Optical inspection showed that the edge of the crack line has sub micrometer roughness. The location of the crack line had no correlation to the etched channel. Hence the etched channel did not pin down the breaking location of the wafer. However, the smoothness of the broken sides is is well below micrometer roughness and straight enough for the positioning of the waveguide entrance 1 μm from the edge. Unlike silicon the GaAs wafer breaks very smooth and straight even without the introduction of a cut (figure 11).

Since the width of the channel was 2 μm, even smaller than the thinnest scribe with a diamond tip, a follow up experiment with a wider channel was done. Also some other channel geometries where used to investigate whether they were more suitable to force the crack to form at the location of the etched channel. The following four geometries where used and wet etching was used to etch 2 μm deep (figure 12):

- Two triangles: The triangle results in a large area etched from the sample surface possibly locally weakening the sample so the crack will form somewhere in the triangle. The triangular shape might then guide the crack propagation in such a way that the crack would emerge at the tip of the triangle and propagate through the sample towards the tip of the other triangle.
- Small triangles connected: The same principle as mentioned above only the etched channel which connects the triangle furthers helps to guide the crack propagation. The crack location is less defined then with the “Two triangle” geometry because of the width of the channel connecting the triangles.
- Big triangles connected: The same as above only the structure is bigger. This could give a indication whether the removal of wafer material weakens the wafer, hence resulting in a crack propagation at that location.
- Straight line: If this profile forces the crack to propagate at the line it also indicates that removing wafer material weakens the wafer such that it forces the crack location. This would also rule out the importance of the introduction of stresses due the deformation of the material with the diamond scribe tip for pinning the crack location.

Three of the four geometries only serve to show the if the crack location can be pinned by etching away wafer material. The channels used, except for the “two triangles”, all have a channel width close to a hundred micrometer.. This already gives the indication that using etched channels to pin down the crack location is not a usable technique.

After cleaving the samples none of the channels succeeded in pinning down the crack location. To help the formation of the crack at the channel a small scribe with the

Figure 13: The edge of a cleaved wafer with a pmma 950 k 4% photoresist spun on its top. The upper gray is the wafer and the blue overshoot is pmma sticking over the edge of the wafer. The white is where the wafer was cleaved and now remains nothing, empty space. The black line is artificial and only serves as a spacer between the picture en the text beneath it.

diamond tip was made at the right side of channel number 3. The hope was that the crack would initiate at the scribed location and would then be guided along the side or through the center of the channel. Although the crack propagated close to a channel side this was most likely not due to the guiding of the channel but simply the cracking of the sample due to the scribed cut. The roughness of the wafer sides was in the order of micrometers and therefore too coarse to position a waveguide entrance.

2.2.6 Cleaving the sample when coated with PMMA

Another option is to first coat the wafer with resist and then cleave it. This results in a layer of photoresist on the edge of the sample with uniform thickness on which a EBL pattering can be burned. Cleaving of the wafer also breaks the photoresist. Although the photoresist breaks much less smooth then the wafer itself it still covers the edge of the wafer (figure 13). No EBL burn tests where performed on these wafer edges. Therefore it is uncertain if the breaking of the photoresist induces stresses or thickness variations which reduce the usability. This method does restrict the number of processing steps to one, since no second layer of resist can be applied after using EBL. Therefore this method is not suitable to create waveguide structure which requires several processing steps to be fabricated.

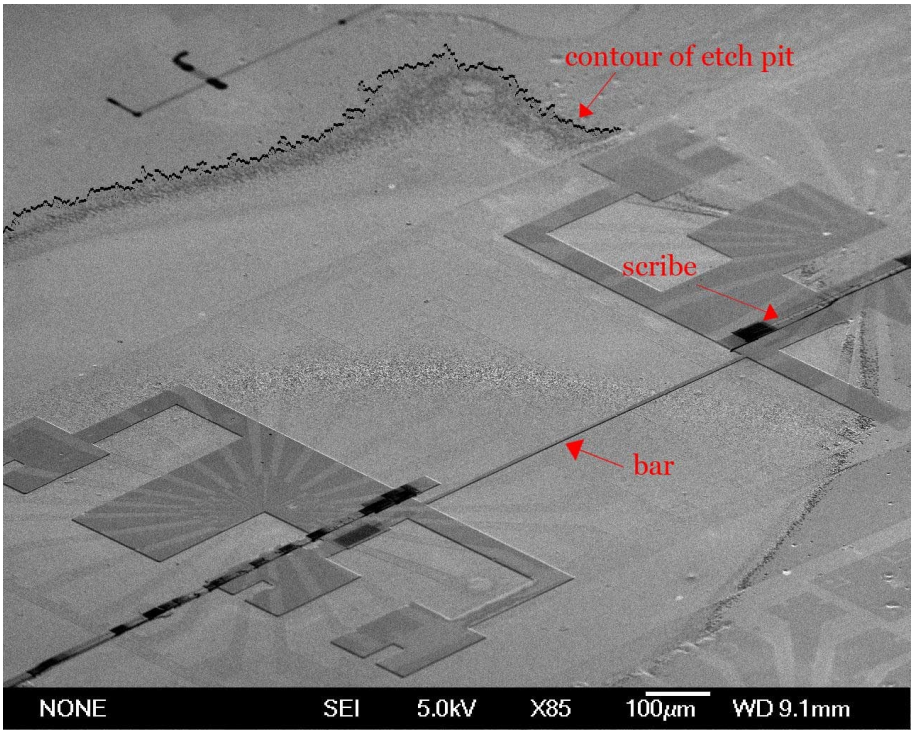

Figure 14: Only the center spot of the wafer developed correctly. A circular shaped valley is seen which has been etched away (indicated by the contour of etch pit arrow). The surrounding wafer has been etched but much less due to the failure of removing the ma-n resist. The SEM picture was taken at a 60 degree angle after etching the wafer.

3 Making the waveguide

Now that there is a process with which we can pin down the cleave location of the wafer up to micrometer precision, a waveguide can be constructed. The first step is to see if it is possible to position an EBL pattern close enough and parallel to the scribed cut.

3.1 Positioning an EBL pattern with respect to the cuts

An old GaAs wafer with a quantum well is used. This wafer has been used before by Maxim Sladkov and shows some structures etched in the wafer. However the height of these structures is on the order of hundred's of nanometers. Therefore it is still possible to coat the wafer with resist and make new structures on top of them. The wafer has a epitaxially grown top layer.

The wafer was spin coated with ma-n 2403, the scribe had no noticeable influence on spin coating. The EBL pattern used was an old design of Maxim Sladkov and the geometry had no other function than to give a reference of how well the EBL pattern could be placed with respect to the scribed cut. The design featured a bar which is positioned parallel and 45 μm away from the side of the cuts closest to the bar. In appendix A.3 the details about the fabrication can be found. The choice of 45 μm is completely arbitrary, it serves purely as a reference to evaluate how precise the pattern will actually be placed with respect to the scribed cuts. For further samples a more useful distance of 1 μm will be used.

After the pattern was written it was developed in ma-D 532. The developing however went problematic. Only a small spot in the center of the wafer developed correctly. Luckily most of the structure was located in this center spot. The rest of the surrounding was still covered with ma-n 2403 and did not dissolve even after a much longer rinsing time in the demi water. Since most of the location exposed by EBL was

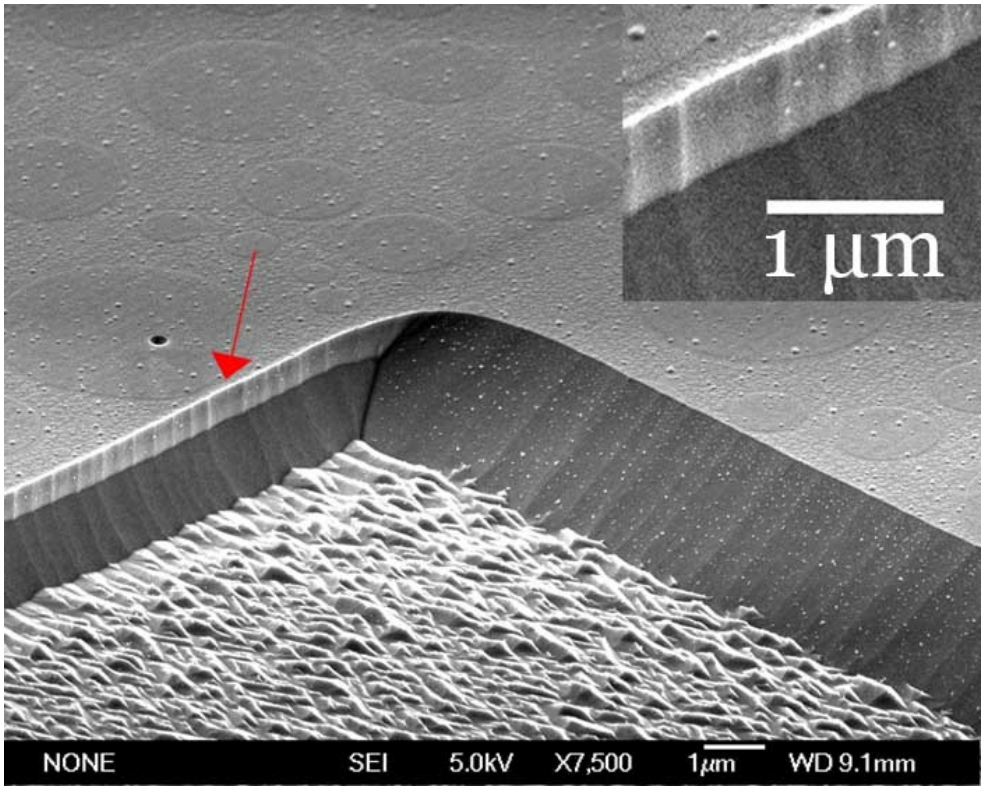

Figure 15: A SEM picture of the side of the bar. There is etching selectivity in crystallographic orientation of the epitaxially grown layer. The arrow points towards the epitaxial layer where etching resulted in a different profile then the GaAs substrate. In the upper left corner this is magnified showing that the roughness is well below the micrometer scale. The etching depth is 1,8 µm.

Figure 16: Cleaving of the sample resulted in a crack propagation deviating only several µm from a straight path. The distance between the bar and the crack is 48,75 µm.

developed correctly the wafer could still be etched (figure 14).

It was etched for 1 minute in a solution of H_2SO_4:H_2O_2:H_2O with concentrations of 1:1:10 respectively. This resulted in a etching depth of 1,8 µm. The bar is positioned 48,75 µm away from and perpendicular to the two cuts. Since the positioning was done without any markers there is a difference of 3,75 µm. This will not pose a problem for the making of more sophisticated devices for which markers can be used. A close up of the bar shows that the etching of the epitaxially grown top layer has a strong dependence on the crystallographic plane being etched. If this dependence is the same for a AlGaAs grown top layer it would allow for a waveguide with a flat entrance and sloped sides. We do not see the plateau formation as we saw with the etched grooves. The reason for this is not clear but it is most likely related to the small channel nature of the grooves which is not present in figure 15. Only larger surfaces are etched. The SEM inspection also allows for a quick estimate of the waveguide entrance roughness. Judged on figure 15 the order of roughness of the side of the bar is below the micrometer scale. This is important since the texture roughness of the waveguide entrance has to be well below the wavelength of the laser beam for a good coupling between the laser and the waveguide. The roughness

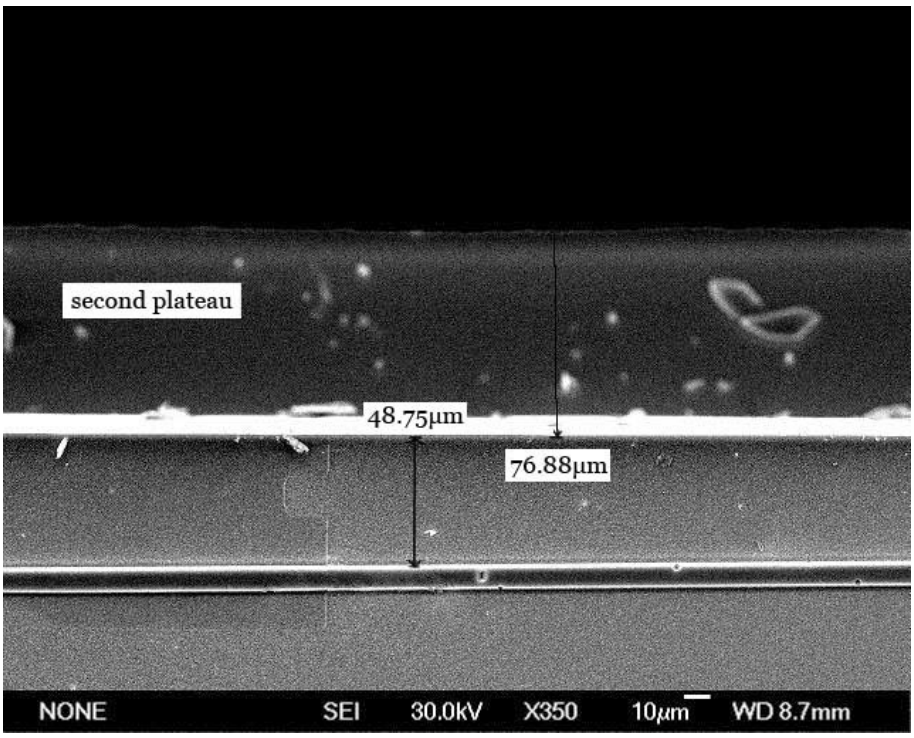

Figure 17: The initial breaking location was at 48,75 µm from the bar. However, the SEM picture clearly shows a second plateau which extends 76.88 µm from the initial crack location and lays much lower then the substrate surface.

of the etched substrate is much higher and close to half a micrometer as can be seen at the bottom of figure 15. Since the etching roughness is heavily depended on the relative concentration of H_2SO_4:H_2O_2 it is very likely a much smoother surface can be obtained **[1]**.

Cleaving the sample resulted in a very straight crack propagation (figure 16). Although there is some deviation, this can also be due to a small misalignment of the two cuts. After further inspection in the SEM it showed that the cleave did not result in breaking the wafer at the same place over the total depth of the sample (figure 17). This could present a problem if the second plateau lies very close to substrate surface. The deviation in cracking location over the depth of the substrate has only be noticed with this wafer, however, the other wafers where only inspected with a optical microscope. This problem could therefore be much more frequent.

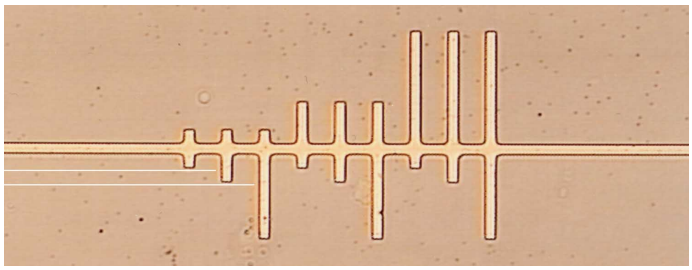

Figure 18: Optical inspection with a microscope of the gold gate which is used as a etching mask for the waveguides. The central bar is the gate backbone. The rectangles orthogonal to the gate backbone are the waveguides. The white lines are inserted as an visual aid. To show the two possible breaking locations of the wafer when it is cleaved.

3.2 The waveguide geometry

After some consultation with Caspar van der Wal a geometry for the waveguide was chosen (figure 18). The area between the two white lines are the two sides of the cut and correspond with the two possible locations where the breaking of the wafer is predicted. The waveguides entrances, bottom side of the picture, have three different lengths.

The 5 μm entrance is useful when the sample breaks at the upper white line and will be situated 1 μm away from the sample edge. The 10 μm entrance is useful if the sample breaks at the bottom line and will be situated 3 μm away from the sample edge. At least one of the waveguides should also be cleaved in two parts so a SEM inspection can show the quality of the waveguide end-face. If the cleaving of a waveguide results in a usable entrance, the positioning of the waveguide with respect to the scribes would be much easier. The unneeded part of the waveguide could be cleaved off instead of the need to cleave away the GaAs bulk material as close as 1μm from the waveguide entrance. The third waveguide is long enough to be cleaved in two parts, independent of both possible breaking locations ensuring a cleaved waveguide is produced.

The varying lengths of the back ends of the waveguides are there to investigate the influence of the length of the waveguides on the propagation of the light inside the waveguides. The width of the waveguides is more or less arbitrary with 3 μm being close to the minimum width possible. In the final experiment a waveguide with a much greater width to hight ratio will be used resulting in a planar, instead of a channel, waveguide. The back bone of the gate, orthogonal to the waveguides, also has a width of 3 μm.

The initial idea was to make the gold gate as high as possible so it could serve as a wall which would block the overshoot of the laser beam. Since the beam would probably be broader than the waveguide entrance it could leak around it and reach the observing end thereby interfering with the measurements. However making a very high gate introduces some extra problems. Since this potential problem is not relevant until the far future it was decided to first make a normal sized gate. For the fabrication process see appendix A.4

3.3 Using the gold gate as etching mask

In an experiment of another FND group member, Ji Liu, a gold gate was used as an etch mask. This approach reduces the number of EBL steps needed and guarantees a perfect match of the gate on the waveguide.

However, a complication arose due to the need of a much deeper etching depth of 1.8 μm and the comparatively small width of 5 μm of the waveguides compared to the Ji Liu experiment. Wet etching is an isotropic etching process and even though for GaAs the etching rates depend on the different crystallographic planes, i.e. wet etching of GaAs will show anisotropic etching, there will be a considerable under etching of the gold gates. Indeed, after wet etching an under etch comparable with the depth of etching was observed. Although the under etch rate is lower than lateral etching due to the shielding of the gold on the top side of the waveguide, there still was an under etch of more then 1,5 μm. This results in the loss of contact surface between the waveguide and the gold gate. Due to the loss of this adhesion the gold starts to curl (figure 20). The resulting waveguides are in the

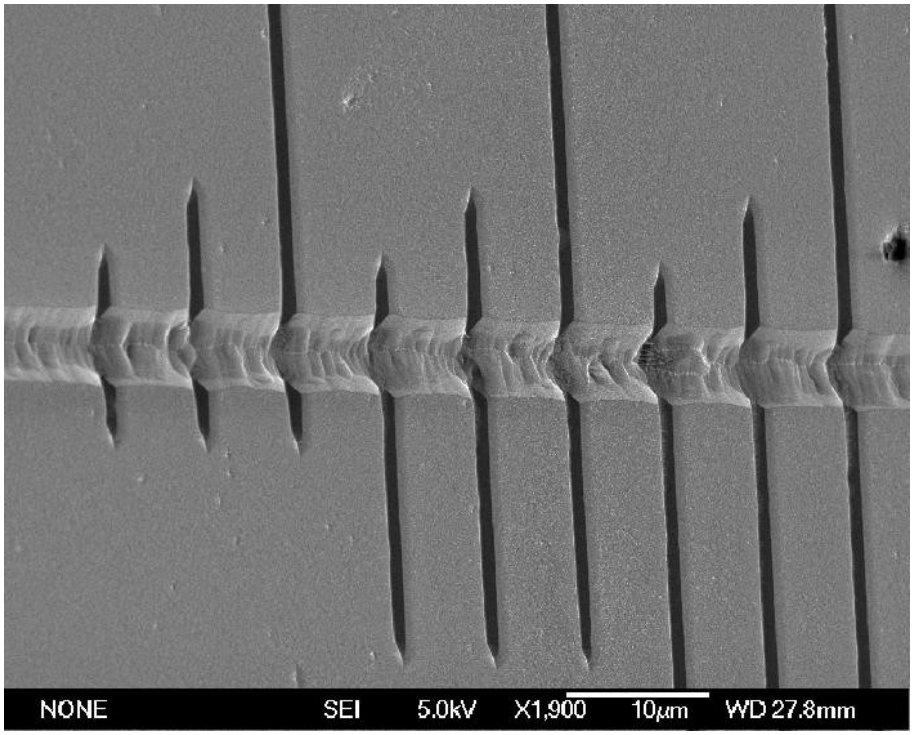

Figure 19: After dry spinning the waveguide the gold gate was completely removed from one of the three waveguides. The remains of the waveguides are rib shaped walls. The The angle under which the image is taken is 60 degrees.

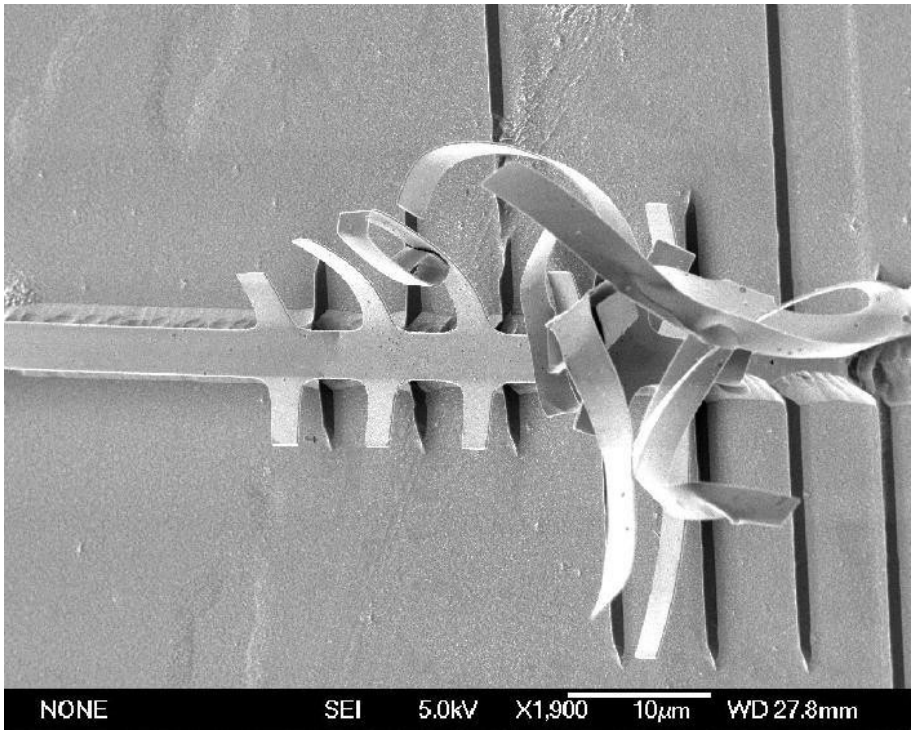

Figure 20: The gold gate curls and bends due to the of loss of contact surface with the waveguides.

form of triangular ridges with a height equal to the etching depth. The etching rate dependence on the crystallographic plane is clearly visible. The long gate, perpendicular to the waveguides, is etched much less steep (figure 19). The long gate backbone has a very

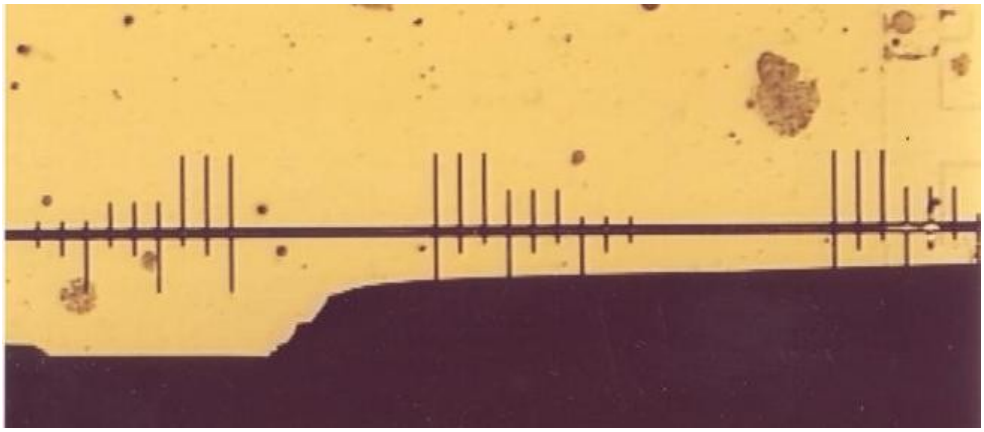

Figure 21: Cleaving of the sample with the failed waveguides resulted in a crack propagation which deviated considerably from a cracking propagation collinear with a [110] direction.

Figure 22: A zoom of the right most waveguide structure of the top picture. The cracking propagation also deviates from a path collinear with the lateral gate indicating the scribe was not made collinear to one [110] direction.

rough texture as if it was etched not only from the sides but also from the top, through the gold mask. This might be due to the use of titanium as an adhesion metal between the wafer and the gold. If the titanium is oxidized by the H_2O_2 it could be dissolved by H_2SO_4, if so another adhesion metal should be used. If the adhesion metal is no longer soluble the gold mask might give the same protection as the ma-n used for the structure in figure 14. However, the ratio of the width of the waveguides to the etching depth is very low and it is therefore not very likely an isotropic etchant can be used for such ratios. The crystallographic depended etching profile in figure 15 might be used to create waveguides with steep, instead of sloped, sidewalls if this effect also shows for the epitaxially grown waveguide layer.

The bar in figure 14 had an etching mask with a width of 10 µm and resulted in a width of 9,25 µm after etching. This suggests that a usable mask width to etch depth ratio can be at least as small as 5:1. The ma-n resist also shows no etching of the surface under the mask, unlike the gold mask. Therefore it might be possible to get a lower mask width to etch depth ratio but it is not very plausible that a ratio of 2:1 can be obtained.

3.4 Cleaving the Waveguide

After cleaving we can see the crack propagation through the unscripted part of the wafer deviated from a collinear path with the scribe (figure 21). The crack started to propagate on the right side of the wafer and propagates smoothly up to two thirds of the wafer shown in figure 21. It can clearly be seen that although the propagation is smooth it is not collinear with the waveguide structure. The reason for this is most likely that the scribe which is made collinear with the waveguide structure had a mis angle with the <110> direction of the wafer. Since the <110> direction is the favorable plane for GaAs to crack the crack started to propagate in that direction instead of the scribe direction. At two thirds from the right we see a major deviation of the cracking which then settles again in the favorable <110> direction. It is not certain why this has happened. Figure 22 is a zoom in of the most right waveguide structure where the mis angle is clearly visible.

4 Conclusion

Cleaving of Silicon wafers proved to be much more difficult then cleaving of GaAs wafers. In GaAs wafers the crack propagates almost entirely in a straight line towards the second cut. The crack propagation in silicon wafers, however, depends heavily on the depth of the cuts which where made to pin down and initiate the crack. The deeper the cut the more the crack will bend away from a straight line. A single scribe resulting in a scratch width of approximately 7 μm is enough to force the wafer to break at the scribed location.

It is possible to determine the cleave location of the GaAs wafer with micrometer precision with the use of a scribed cut made by a diamond tip. The sides of the unscripted part of the wafer showed, after cleaving, a roughness well below the micrometer scale. This roughness allows for the placing of the waveguide entrance less then 1 μm from the edge. The positioning of the scribe it self can be done with a precision in the order of micrometers. However, the positioning could be enhanced by outfitting the Scriber with a microscope which has a higher magnification.

The straightness of the crack propagation through the wafer most likely depends on how well the initial scribe was made with respect to a {100} direction of the wafer. The breaking location of the wafer always forms at one of the sides of the scratch, however, no evidence could be found the wafer will break at one side of the scratch specifically. Therefore there are two possible location where the wafer will break. This should be kept in mind when designing the waveguide structures.

The etched channel method did no result in pinning of the crack location. Although the GaAs wafers broke, the crack location was not related to the etched channels.

It is possible to cleave wafers which are already covered with a photoresist. The photoresist stick over the edge of the wafer and is consistently covering the whole wafer over lengths of more then 100 micrometers, if the photoresist is still usable for EBL has not been tested. .

Although the scribed cut process is very consistent a wafer could break badly. Because the cleaving of the wafer will be done after all the processing steps, a device could be destroyed or be unusable. The cleaving however always results in a crack at the designated location. Bending of the crack propagation of the wafer is observed but stays below a deviation of maximally several micrometers over a length of a millimeter. Although there is uncertainty on which side of the scribe the wafer will break, the break will be amazingly close to the edge of the scribe making it possible to place a waveguide structure with EBL at least as close as 1 μm from the predicted crack location.

After etching a wafer with a epitaxially grown GaAs top layer there is a clear crystallographic etching dependence visible. This dependence could be used to create a waveguide with a flat entrance or with flat sides. The roughness is well below the micrometer but could most likely be much lower by changing the relative concentrations of H_2SO_4:H_2O_2 **[1]**. Inspection of the sample showed that the wafer, although cleaved at the right location in the top part of the wafer, did not break at the same location through the depth of the sample. If this occurs frequently is unclear since only two samples where made and inspected in the SEM. The depth at which the breaking location starts to deviate is not determined. This deviation could cause blocking of the input beam.

Making waveguides by using gold as an etching mask failed. This was most likely due under etching since the ratio of the width of the waveguides to the etching depth is very low (3:2). It is unlikely an isotopic wet etchant can create well defined structures with such ratios. since there will be considerable under etching. Etching with a ma-n 2403 photoresist showed that a ratio of (10:2 in μm) results in an total under etch (i.e. from both sides) of 0,75 μm. Pre-etching the samples with sulfuric acid, which is highly diluted with demi water, will clean the samples surface from any surface oxides resulting in better adhesion of photo resists and metals.

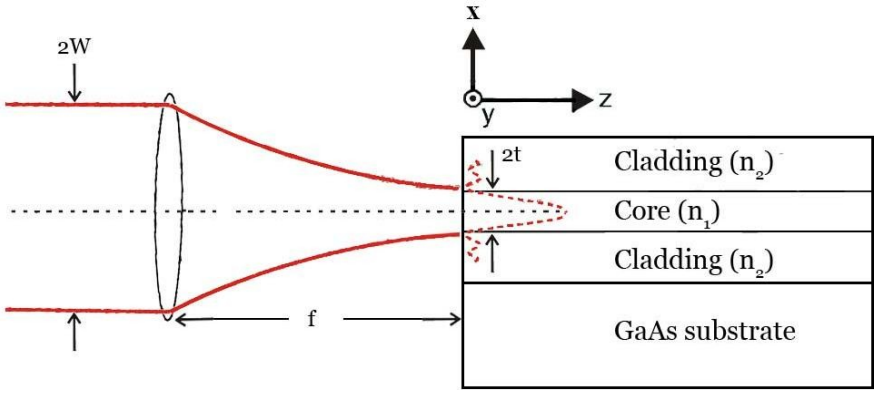

Figure 23: end-fire coupling method. The incident beam has a Gaussian profile as depicted by the dotted line.

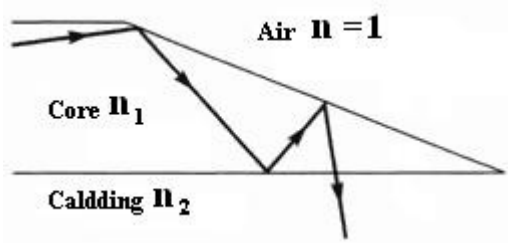

Figure 24: Tapered output of the waveguide

5 Planar Waveguide Theory

In appendix B a detailed analytical derivation of the TEM fields propagating inside a symmetrical planar[2] dielectric waveguide. In this section some characteristics of the waveguide are investigated.

5.1 Input/output coupling of the waveguide

Coupling a laser beam into the waveguide end-face with the use of a lens is called end-fire coupling. The scattering losses at the end face can be very low if the end-face is polished to a optically smooth finish. This can be done by etching or by cleaving the waveguide. Transferring the beam energy to a mode in the waveguide is accomplished by matching the field of the mode in the waveguide by the beam field. The fraction coupled from the fundamental mode of the laser to mode S of the waveguide is give by [2]:

$$|A_S|^2 = \left(\frac{8}{\pi S}\right)^2 \frac{n_L n_S}{(n_L+n_S)^2} \cos^2\left(\frac{\pi t_g}{2t_L}\right) \frac{1}{[1-(t_g/S t_L)^2]^2} \left(\frac{t_g}{t_L}\right) \quad S = 1,3,5\ldots \quad (1)$$

where n_L is the refractive index of the medium from which the laser enters the waveguide, which in this case is vacuum. n_S is the refractive index of the waveguide substrate which is taken as the average of the refractive index of GaAs and AlAs. T_G is the width of the core of the Waveguide and t_L the spot size of the laser beam. Since the lowest mode has a Gaussian distribution it is easy to match with a laser beam which also has a Gaussian distribution.

For optimal coupling the beam diameter must be closely matched to the waveguide diameter with the use of a lens. For a Gaussian beam having width W the beam must be focused into a width $2t = \lambda f/(\pi 2W)$ by a lens with focal length f (Figure

[2]The type of waveguide in this thesis is a channel waveguide, i.e. there is a boundary in the y-direction ($L_x \approx L_y$), and so $\partial/\partial y \neq 0$ in the wave equation. However, the waveguide which will be used in the final experiment will most likely be planar therefore only the planar waveguide theory is discussed.

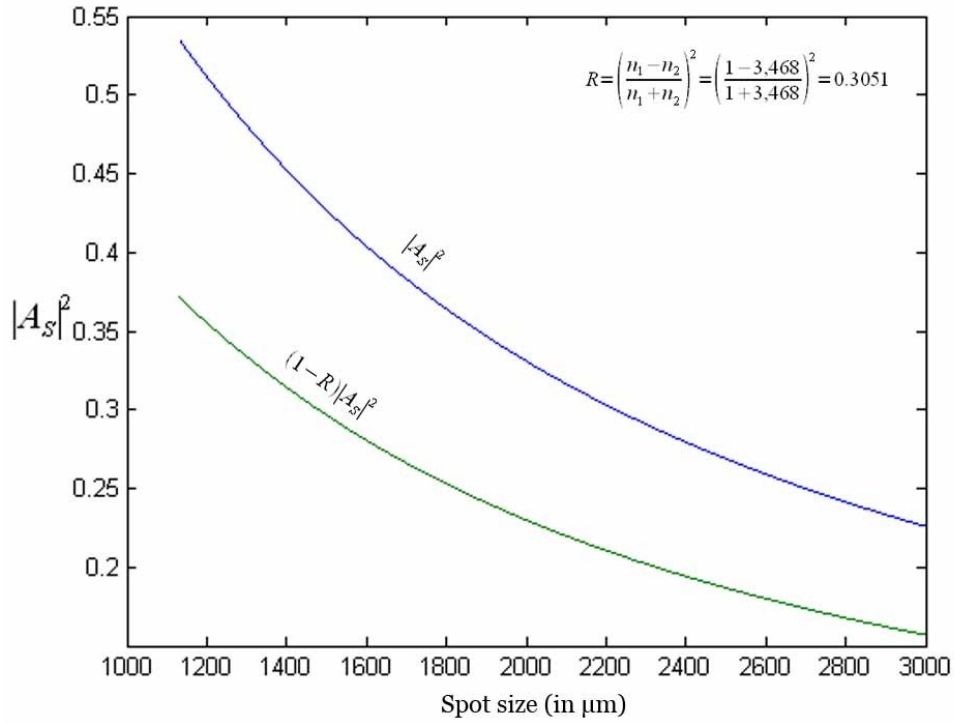

Figure 25: A plot of the coupling efficiency of the waveguide versus the spot size of the incident laser beam. $|A_s|^2$ represents the coupling efficiency without Fresnel reflection and (1-R) $|A_s|^2$ represents the coupling efficiency with Fresnel reflection at the waveguide input facet.

23). The theoretical minimum spot size obtainable in the cryostat is 1.13 μm which is almost double the size of the waveguide core width. The corresponding coupling efficiency with this spot size is calculated to be 0.3702. The coupling is further decreased by Fresnel reflection loss at the end-face of the waveguide. For a Detailed description see Appendix C. Aligning and focusing the beam becomes problematic when using single mode waveguides which have a thickness in the order of 1 μm. The theoretical calculated values of the coupling efficiency are calculated with the use of equation 1. The result is plotted in figure 25 where the coupling efficiency is a function of the beam diameter. The coupling efficiency is very sensitive to misalignment especially in the lateral direction and has to be tuned up to 0.1 μm spatial resolution for optimal result. The output of the waveguide also suffers from Fresnel reflection. Having a tapered waveguide exit reduces the amount of back scattering waves and might thereby increase optical power output of the waveguide (figure 24)**[3]**.

5.2 Excitable modes in the waveguide

As is derived in Appendix B.3 the number of modes that are sustained by a waveguide is given by

$$M=\frac{2\mathrm{d}}{\lambda_0}\sqrt{n_1^2-n_2^2}=\frac{2\cdot 0.6}{0.8}0.58=0.87 \qquad (2)$$

For the waveguide used in this research we have d= 600 nm, λ_0=800 nm, n_1=3.468 and n_2=3.4185 where the refractive indices are taken from **[4]** and **[5]**. Therefore this waveguide can sustain 1 mode. Since the waveguide is symmetrical, the upper cladding has the same refractive index as the lower cladding, hence there is no cut-off wavelength for the fundamental modes TE_0 and TM_0 and these modes are therefore always excitable. To obtain the highest possible optical power inside the QW it is most favorable to only excite the fundamental Gaussian shaped mode. This distribution has the largest amplitude at the

center of the waveguide core. Since the waveguide can only sustain the lowest mode any power coupled into other modes will leak from the waveguide. This is because any mode which is not sustained will not be total internal reflected and therefore will leak out of the system whit each successive reflection at the waveguide core boundaries. Due to the Gaussian beam shape of the laser it should not prove difficult to excite only the fundamental modes. It is however crucial to have a laser beam which has the same Gaussian shape as the lowest mode of the waveguide to obtain appreciable coupling efficiencies.

5.3 Single waveguide mode coupling

Any possible mode coupling is important since the waveguide only sustains the fundamental mode. Therefore any mode coupling will result in loss of optical power since it will leak out of the waveguide. Since the modes of a waveguide are orthogonal the power carried by a mode cannot be transfered to another mode. Therefore the modes excited inside a waveguide will propagate through the waveguide independently and hold the initial distribution. To describe the coupling between optical waves a certain polarization ΔP has to be included in the wave equation

$$\nabla \times \nabla \times \boldsymbol{E}(\boldsymbol{r},t) + \mu \epsilon_0 \frac{\partial^2 \boldsymbol{E}(\boldsymbol{r},t)}{\partial t^2} = \mu \frac{\partial^2}{\partial t^2} \boldsymbol{\Delta P}(\boldsymbol{r},t) \qquad (3)$$

We assume ΔP to be small compared with the electric field and is therefore treated as a perturbation of the linear, static properties of the medium. We are not concerned with the coupling of modes between different waveguides by evanescence fields. This leaves coupling modes in the same waveguide by longitudinally homogeneous perturbations, and co- and contra directional coupling by longitudinally inhomogeneous, usually periodical perturbations.

Coupling of a optical wave with different frequencies is only possible if the optical properties of the medium in which the optical wave propagates is time varying or optically non linear. Time varying optical properties can be induced by time varying electric, magnetic and acoustic fields through electro-optic,magnetic-optic and acousto-optic effects resulting in TE ↔TM mode conversion. Any dielectric perturbation Δε(x,y,z) , in this case due to waveguide side wall imperfections, could also result in coupling of the modes. This will most likely be no problem since the waveguide core is sandwiched between epitaxially grown cladding and therefore the cladding-core interface has a very homogeneous profile. If a channeled waveguide is produced the side will have roughness due to etching and could cause mode coupling. Also non-linear effects like second-harmonic generation, and optical parametric oscillation could result in the coupling of different waveguide modes **[6]**. It is difficult to predict any possible mode coupling for the waveguide in this research and no simple theoretical prediction can be made.

5.4 Distribution of guided modes and group velocity

Dispersion in dielectric waveguides has three different causes. First we have material dispersion which is dispersion caused due to the frequency dependent refractive index of the material. The second cause is mode dispersion which is due to the different group velocities of the modes them selfs. The evanescent waves of higher modes penetrate deeper into the cladding and therefore travel faster. Finally we have waveguide dispersion which causes a variation in group velocity even within one mode. This last cause is normally small compared to the other two and will be ignored **[7]**.

The group velocity can be derived from the following two relations which where derived in appendix B.3. Only mode dispersion is calculated since material and waveguide dispersion are much smaller.

For the TE modes

$$hd - \frac{m\pi}{2} = \arctan\left(\frac{p}{h}\right) \quad \text{With} \quad \begin{matrix} h = \sqrt{(k_0^2 n_1^2 - \beta^2)} \\ p = \sqrt{(\beta^2 - k_0^2 n_2^2)} \end{matrix} \tag{4}$$

Where n is the corresponding index of refraction for cladding or core and β is the propagation constant from the wave equation.

and for the TM modes

$$hd - \frac{m\pi}{2} = \arctan\left(\frac{n_1^2}{n_2^2}\frac{p}{h}\right) \tag{5}$$

The group velocity is the given by $\upsilon = d\omega/d\beta$. Using $k_0 = \omega/c$ we then get **[8]**

$$\upsilon_g = \frac{d\,\tan(\theta) + \frac{\partial \phi}{\partial \beta}}{\frac{n_1 d}{c_1 \cos(\theta)} - \frac{\partial \phi}{\partial \omega}} \tag{6}$$

The terms $\partial\phi/\partial\beta$ and $\partial\phi/\partial\omega$ represent the penetration of the wave into the cladding of the waveguide which is know as the Goos-Hänchen effect.

We now determine those two terms **[9]**

$$\frac{\partial \phi}{\partial \beta} = \frac{\beta(h^2 + p^2)}{hp(n_1^2 - n_2)k_0} \tag{7}$$

and

$$\frac{\partial \phi}{\partial \omega} = -\frac{h^2 n_2^2 + p^2 n_1^2}{\omega hp(n_1^2 - n_2^2)} \tag{8}$$

Appendix A

Device fabrication

All fabrication procedure for the devices that were used in this theses will be described here.

A.1 Etched rectangular Channel

Channel geometry: width 2 μm, length 700 μm

1. Clean the wafer in boiling acetone for 10 minutes
2. Use ultrasonic bath at default settings for 10 seconds, rinse with IPA
3. Spin the wafer dry
4. Spin 70 nm 950K PMMA (2% in Ethyl lactate) at 4000 rpm for 60 seconds
5. Bake for 15 minute at 180 °C
6. After EBL develop in 1:3 MIBK / IPA for 60 seconds
7. Rinse with IPA for 30 seconds
8. Etch in 1:1:50 H_2SO_4:H_2O_2:H_2O solution for 1 min (estimated etching speed 2 nm/s)

A.2 Etched four geometries on one wafer

The same procedure as in A.1 is used. The only difference is in step 8 where a etch solution of 1:1:10 H_2SO_4:H_2O_2:H_2O is used. The wafer was etched for 1 minute which should result in a depth of 2 μm.

A.3 Bar

There where some troubles in obtaining a wafer with a usable spun resist profile. The initial recipe failed to form a flat layer on top of the wafer. The profile was very speckled, some pieces of the wafer where covered with resist while other parts had barely any resist on it.
Successful Recipe

1. Clean the wafer in boiling acetone for 10 minutes
2. Use ultrasonic bath at default settings for 10 seconds, rinse with IPA and Methanol
3. Pre-bake the wafer for 2 minutes on a hotplate at 200 °C
4. Spin the wafer with the spinner to set the right rpm and cool the wafer.
5. Apply HMDS at 3000 rpm for 30 seconds.
6. Spin the ma-n 2403 at 3000 rpm for 30 seconds (resist thickness: 350nm).
7. Bake at 90°C for 60 seconds (hot plate). If required, the etch resistance and thermal stability of the resist can be increased by applying a higher prebake temperature (max. 110 °C) or a longer prebake time. The developing time will increase in this case.
8. Develop in ma-D 525 for 4 minutes, immediately followed by rinsing in deionized water for approximately 5 minutes. Spin dry at 3000 RPM for 30 seconds.
9. Lift-off : Ready-to-use removers mr-Rem 660 (solvent based) and ma-R 404/S (strongly alkaline) are recommended. Acetone, N-methylpyrrolidone (NMP) or oxygen plasma is also suitable for the residue free removal of the resist.

A pre-baking time of 10 minutes in a oven was used at first but did not result in a good photoresist film on the wafer. Baking the sample for at least 60 minutes resulted in a much better photoresist profile on the wafer. Baking the sample on a hot plate considerably lowers the amount of time needed. The developing still went problematic. This problem is

however solved by another group member. The developing time should be extended to about 4 minutes.

The alignment of the pattern which has to be written with EBL was done in two steps:

Angle correction

1. The beginning of one of the scratches has to be located. Read the coordinates needed for the angle correction. Use one of the sides of the cut as your angle correction and not the center since the crack will propagate at the one of the sides of the cut. This will make positioning the EBL pattern easier.
2. Move to the other side of the sample and follow the same procedure with the second scratch. The execute the angle correction.

Origin Correction

1. The width of the sample at the scratch location was measured with the use of the Scriber. Then the length of the two cuts were measured and hence the center of the unscribed gap could be calculated. The precision of the measurement is in the order of micrometers.
2. An origin correction was then executed with respect to the side of the sample at the scratch location.

A.4 Using a gold layer as a etching mask

All preliminary steps are the same as the recipe used in A.1. Two different photoresist where used. The first recipe was taken from FND group member Erik Koops:

Recipe one

- 400 nm 50 K PMMA (9% in Chlorobenzeen) – 4000 rpm (60 seconds)
- 70 nm 950 K PMMA (2% in Ethyl Lactate) – 4000 rpm (60 seconds')
- bake at 180 degrees Celsius for 15 minute in oven

This recipe was chosen because it was possible to make a thicker gold layer to serve as an laser overshoot blocker. Also the double resist layer would facilitate a much easier lift-off. The problem with this recipe was the use of the very sensitive 50 K PMMA layer. Since the scribe had to be found by visual inspection the 50 K PMMA covering the scribes is exposed. The electrons charged and deformed the 50 K PMMA so heavily that visual inspection became impossible. It was therefore impossible to position the EBL structure with respect to the scribed cuts. This problem was partly overcome by switching to the smallest aperture, a 10 μm aperture, so the PMMA would be exposed less. However the benefits of an easier lift-off are not needed for this particular structure.

Recipe two

- 400 nm 950 K PMMA (4% in Etyl Lactate) – 3000 rpm (60seconds)
- bake at 180 degrees Celsius for 15 minute in oven

For the burning of the structure the initial aperture used was 120 μm. Since the cuts have to be found by exposing the resist covering them, this aperture size made it more difficult to observe the cuts. Therefore a switch was made to the 30 μm aperture which did not significantly increase the burning time.

After burning the EBL pattern the photoresist is developed dissolving all the resist which was exposed in the EBL step. The mask has to be created in such a way that the desired waveguide pattern is not covered with photoresist. The next step is to deposit a 5 nm layer of titanium, for adhesion of the gold, and on top of this layer a 180 nm layer of gold with the Temescal e-beam evaporator. Finally all PMMA will be removed during the lift-off and only the gold layer which was deposited on the exposed wafer parts will remain. After etching, the complete wafer will be etched except for the part under the gold layer resulting in channel waveguides with a height of the etching depth of the surrounding material.

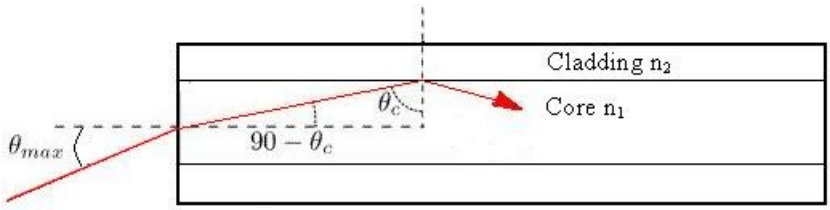

Figure 26: Total internal reflection and acceptance angle $\theta_a = \theta_{max}$.

Appendix B

Derivation of the Field Distribution inside a Symmetrical Planar Waveguide

B.1 Total Internal Reflection

Total internal reflection is the reflection of a ray at the boundary between two dielectric materials where there is no transmission of the ray off light into the outer material. Two conditions have to be satisfied for a light ray to be totally internal reflected.

1. The refractive index of the core n_1 has to be higher then the refractive index of the cladding n_2
2. The ray has to strike the boundary between the materials with a angle larger then the critical angle $\theta_c = \sin^{-1}\left(\frac{n_2}{n_1}\right)$

On the left side of figure 26 a waveguide is shown where a ray strikes the waveguide entrance. The acceptance angle θ_a is the angle for the cone of rays accepted by the waveguide and can be expressed by the numerical aperture (NA) of the waveguide which is given by .

$$NA = \sin(\theta_a) = \sqrt{n_1^2 - n_2^2} \tag{9}$$

B.2 Solution of the Wave Equation

This derivation is an adaptation of the derivation done in [10] for a asymmetric waveguide. The aim is to describe how the laser, which is considered to be a classical transverse-electromagnetic (TEM) wave, behaves inside a waveguide giving insight into the mode structure, power confinement and propagation properties of the wave . In a waveguide a TEM plane wave is propagated along the guide while it transverse spatial distribution is maintained. We assume that all media are homogeneous, isotropic, linear, stationary and non-dispersive. Also the waveguide extends to infinity in the y and z directions. We let the TEM plane wave propagate in the z direction of the waveguide therefore the electromagnetic fields become

$$\boldsymbol{E}(\boldsymbol{r}, t) = \boldsymbol{E}(x, y)\mathrm{e}^{j(\omega t - \beta z)} \tag{10}$$

$$\boldsymbol{H}(\boldsymbol{r}, t) = \boldsymbol{H}(x, y)\mathrm{e}^{j(\omega t - \beta z)} \tag{11}$$

The modes of a waveguide are a solution of the wave equation and therefore satisfy the Helmholtz equation

$$(\nabla^2 + k_0^2 n_i^2)\boldsymbol{E}(\boldsymbol{r}) = \frac{\partial^2}{\partial x^2}\boldsymbol{E}(x,y) + (k_0^2 n_i^2 - \beta^2)\boldsymbol{E}(x,y) = 0 \tag{12}$$

$$(\nabla^2 + k_0^2 n_i^2)\boldsymbol{H}(\boldsymbol{r}) = \frac{\partial^2}{\partial x^2}\boldsymbol{H}(x,y) + (k_0^2 n_i^2 - \beta^2)\boldsymbol{H}(x,y) = 0 \tag{13}$$

Where k_0 is the wavenumber in vacuum and we used $\partial/\partial y = 0$ and $\partial/\partial z = -j\beta$ since the waveguide is uniform in the y and z direction. And n_i is the refractive index of the core (i=1) or the cladding (i=2).

And we have the Maxwell equations

$$\nabla \times \boldsymbol{E} = -\mu_0 \frac{\partial \boldsymbol{H}}{\partial t} \tag{14}$$

$$\nabla \times \boldsymbol{H} = \epsilon_0 n^2 \frac{\partial \boldsymbol{E}}{\partial t} \tag{15}$$

Where we assume $\mu_r = 1$ since we are dealing with non magnetic materials so $\mu = \mu_0$ and $\varepsilon = \varepsilon_0 n^2$.
If we now substitute equations (10) and (11) into the Maxwell equations we obtain:

1) The transverse electric (TE) mode where the electric field is orthogonal to the plane of incidence.

$$E_y = \frac{\omega\mu}{\beta} H_x \tag{16}$$

$$\frac{\partial E_y}{\partial x} = -i\omega\mu H_z \tag{17}$$

$$E_x = E_z = H_y = 0 \tag{18}$$

2) The transverse magnetic (TM) mode where the magnetic field is orthogonal to the plane of incidence.

$$H_y = \frac{\omega\epsilon}{\beta} E_x \tag{19}$$

$$\frac{\partial H_y}{\partial x} = \frac{-\omega\epsilon}{i} E_z \tag{20}$$

$$H_x = H_z = E_y = 0 \tag{21}$$

The field distribution in the waveguide has to be chosen and this can be done with the help of equation (12). From equations (2) and (3) we know $k_0 n_2 < \beta < k_0 n_1$ so

$(\frac{1}{E_x})\frac{\partial^2}{\partial x^2} = \beta^2 - k_0^2 n_1^2 < 0$ inside the core and therefore the solution is sinusoidal and

$(\frac{1}{E_x})\frac{\partial^2}{\partial x^2} = \beta^2 - k_0^2 n_2^2 > 0$ inside the cladding and therefore the solution is exponential. Since the fields must match at the core-cladding boundary at all points the

fields in the cladding have to vary with z as $exp(-i\beta z)$. To obtain a physical possible solution we assume the field is a decaying exponential in the cladding.

We take E_y in the form

$$\boldsymbol{E}_{\boldsymbol{y}}(x,y,z,t)=\mathcal{E}_y(x)\,e^{j(\omega t-z)} \tag{22}$$

The electric field distribution, polarized in the y direction, is then chosen as follows

$$\mathcal{E}_y(x)=\begin{cases} A\,e^{-p(x-t)} & t\leqslant x<\infty \\ B\cos(hx-\phi) & -t\leqslant x\leqslant t \\ C\,e^{p(x+t)} & -\infty\leqslant x<-t \end{cases} \tag{23}$$

And its derivative towards x then becomes

$$\frac{\partial \mathcal{E}_y}{\partial x}=\mathcal{H}_z(x)=\begin{cases} -Ap\,e^{-p(x-t)} & t\leqslant x<\infty \\ -Bh\sin(hx-\phi) & -t\leqslant x\leqslant t \\ Cp\,e^{p(x+t)} & -\infty\leqslant x<-t \end{cases} \tag{24}$$

The wavenumbers h, in the core, and p, in the cladding, can be found by substituting equation (19) into (12)

$$h=\sqrt{(k_0^2n_1^2-\beta^2)} \tag{25}$$

$$p=\sqrt{(\beta^2-k_0^2n_2^2)} \tag{26}$$

We now use the boundary conditions that the tangential components $\mathcal{E}_y$ and $\partial\mathcal{E}_y/\partial x=\mathcal{H}_z$ have to be continues across the core-cladding boundary.

Which gives for $\mathcal{E}_y$

$$\begin{aligned} A&=B\cos(ht-\phi) && x=t \\ C&=B\cos(ht+\phi) && x=-t \end{aligned} \tag{27}$$

And for $\mathcal{H}_x$

$$\begin{aligned} Ap&=Bh\sin(ht-\phi) && x=t \\ Cp&=Bh\sin(ht+\phi) && x=-t \end{aligned} \tag{28}$$

Using equation (28) to divide the constants A and B out of (27) we get the relation

$$\left.\begin{aligned} pt\cos(ht+\phi)&=ht\sin(ht+\phi)\rightarrow\tan(ht+\phi)=\frac{pt}{ht} \\ pt\cos(ht-\phi)&=ht\sin(ht-\phi)\rightarrow\tan(ht-\phi)=\frac{pt}{ht} \end{aligned}\right\}\tan\left(ht+\frac{m\pi}{2}\right)=\frac{pt}{ht} \tag{29}$$

Where ϕ = mπ /2 with m=0,1,2,.....Using equations (25) and (26) we get the expression

$$(ht)^2+(pt)^2=(kt)^2(n_1^2-n_2^2) \tag{30}$$

Solutions of the dispersion equations for the TE and TM modes are those values of ht and pt which satisfy equations (29) and (30) simultaneously.

Determination of Constant B

Constant B can be determined by evaluating the optical power carried by the waveguide.

$$P = \frac{-1}{2}\int_{-\infty}^{\infty} E_y H_x^* dx = \frac{\beta}{2\omega\mu_0}\int_{-\infty}^{\infty} \left(\mathcal{E}_y(x)\right)^2 dx \tag{31}$$

Which result for the three different fields in

$$P_{core} = \frac{\beta t B^2}{2\omega\mu_0} \tag{32}$$

$$P_{clad} = \frac{\beta t B^2}{2\omega\mu_0}\left(\frac{1}{2\mathrm{p}}\right) \tag{33}$$

The total power is

$$P = P_{core} + 2\mathrm{P}_{clad} = \frac{\beta t B^2}{2\omega\mu_0}\left(1 + \frac{1}{pt}\right) \tag{34}$$

Which results in

$$B = \left(\frac{2\mathrm{P}\omega\mu\, p}{\beta(pt+1)}\right)^{\frac{1}{2}} \tag{35}$$

We can now define the power confinement factor inside the waveguide core

$$\frac{P_{core}}{P} = \frac{pt}{pt+1} \tag{36}$$

This same procedure can be followed for the TM modes and will not be carried out explicitly. We find the following mode restriction:

$$\tan\left(hd + \frac{m\pi}{2}\right) = \frac{n_1^2}{n_2^2}\frac{pt}{ht} \quad \text{Where m=0,1,2,...} \tag{37}$$

To determine the constant we use

$$P = \frac{1}{2}\int_{-\infty}^{\infty} E_y H_x^* dx = \frac{\beta\epsilon_0}{2\omega}\int_{-\infty}^{\infty} \frac{\left(\mathcal{H}_y(x)\right)^2}{n^2(x)} dx \tag{38}$$

Which results in

$$B = \left(\frac{2\mathrm{P}n_1^2 n_2^2 \omega\, p}{\beta\epsilon_0(pt\,n_2^2 + n_1^2)}\right)^{\frac{1}{2}} \tag{39}$$

We can now define the power confinement factor inside the waveguide core

$$\frac{P_{core}}{P} = \frac{ptn_2^2}{n_1^2(ptn_2^2 + n_1^2)} \tag{40}$$

Appendix C

C Fresnel reflection at the end-face

Fresnel reflection for the TE mode is given by (see **[8]** eq. 6.2-4 and 6)

$$r_x = \frac{n_1 \cos(\theta_1) - n_2 \cos(\theta_2)}{n_1 \cos(\theta_1) + n_2 \cos(\theta_2)} \tag{41}$$

and for the TM mode

$$r_y = \frac{n_2 \cos(\theta_1) - n_1 \cos(\theta_2)}{n_2 \cos(\theta_1) + n_1 \cos(\theta_2)} \tag{42}$$

The power reflectance is defined as

$$R = |r^2| \tag{43}$$

If we use Snellius law $(n_1/n_2)\sin(\theta_1)=\sin(\theta_2)$ we find (see **[11a])**

$$R_x = \frac{\sin^2(\theta_1 - \theta_2)}{\sin^2(\theta_1 + \theta_2)} \tag{44}$$

$$R_y = \frac{\tan^2(\theta_1 - \theta_2)}{\tan^2(\theta_1 + \theta_2)} \tag{45}$$

The beam is coupled very close to normal incidence due to the end-fire coupling and the power reflectance at normal incidence becomes

$$R = \left(\frac{n_1 - n_2}{n_1 + n_2} \right)^2 \tag{46}$$

For this specific waveguide we have $n_1 = 1$ and $n_2=3{,}468$ resulting in a power reflectance of R=0.305 %. This reflectance occurs at the entrance face and at the exit face and is therefore a considerable loss. It is possible to reduce this reflectance loss with the help of an anti-reflectance coating. For near normal incidence the net reflectivity is given by (see **[11b])**

$$R = \left(\frac{|n_1 n_2 - n_{ar}^2|}{|n_1 n_2 + n_{ar}^2|} \right)^2 \tag{47}$$

Where n_{ar} is the refractive index of the anti-reflectivity coating.

Acknowledgements

I would hereby like to thank first of all the whole FND group for being able to do my Bachelor research with this great group. I am very grateful to Caspar for giving me the chance to work in this group and for the many useful comments he has given concerning my work. I would like to thank Maksym for his supervision and especially the help in the cleanroom and his comments on the writing of this thesis. All though Maksym explained the basic workings of the EBL machine I would like to thank Bram for helping me out even more with this wretched device.

Bibliography

[1] A. G. Baca, C.I.H. Ashby, Fabrication of GaAs Devices. Institution of Electrical Engineers, 2005. ISBNL: 0863413536 (Wet etching and photolitography of GaAs and related alloys)

[2] Hunsperger, R. G. and Yariv, A. and Lee, A. Parallel end-butt coupling for optical integrated circuits. Applied Optics, Volume 16, Issue 4, Apr 1977 page(s): 1026 - 1032. ISSN 0003-6935

[3] Matt Young. Optics and Lasers: Including Fibers and Optical Waveguides. Springer, 2000. ISBN**:** 354065741X (page 325)

[4] BATOP GmbH Semiconductor optoelectronic devices http://www.batop.de/informations/n_AlGaAs.html

[5] Ioffe physico-Technical Institute http://www.ioffe.rssi.ru/SVA/NSM/Semicond/AlGaAs/

[6] Yariv, A. Coupled-mode theory for guided-wave optics. Quantum Electronics, IEEE Journal of Volume 9, Issue 9, Sep 1973 Page(s): 919 - 933 (mode-coupling)

[7] Clifford R. Pollock, Michal Lipson. Integrated Photonics. Springer, 2003 ISBN:1402076355 (group velocity)

[8] Saleh and Teich. Fundamentals of Photonics. Wiley-interscience, 1991. ISBN: 0-471-83965-5 (Polarization, Electromagnetic Optics and waveguide theory)

[9] Nigel J. Cronin. Microwave and optical waveguides. Taylor & Francis, 1995. ISBN:0750302166 Institute of Physics, Great Britain (group velocity)

[10] A. Yariv and P. Yeh. Optical Waves in Crystals. Wiley-interscience, 1984. ISBN 0-471-09142-1 (wave equation derivation and mode coupling)

[11a] E. Hecht. Optics. Pearson Education Limited, 2003. ISBN: 0321188780. chapter 8 page 351 (Fresnel reflection at the end-face)

[11b] E. Hecht. Optics. Pearson Education Limited, 2003. ISBN: 0321188780. chapter 9 page 428-429 (Fresnel reflection at the end-face)

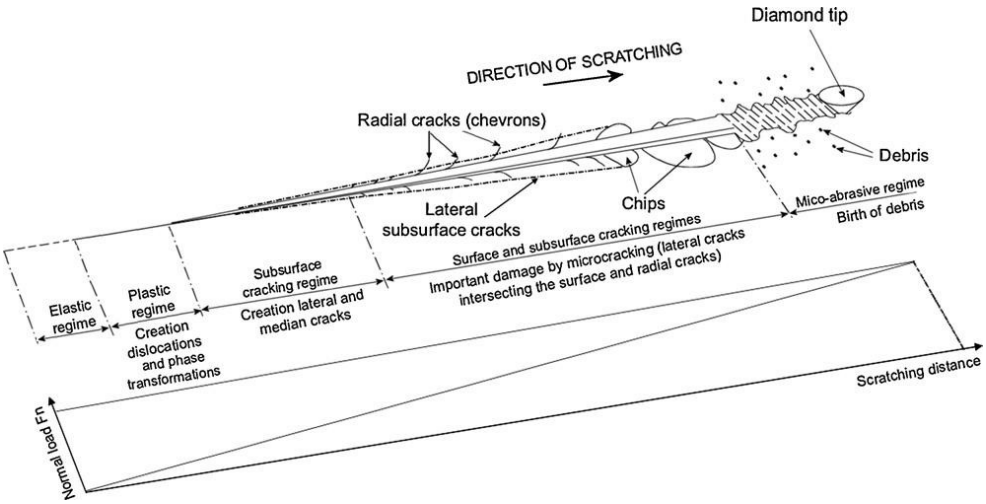

Figure 27: Deformation of the wafer as a function of the loading force of the diamond tip.

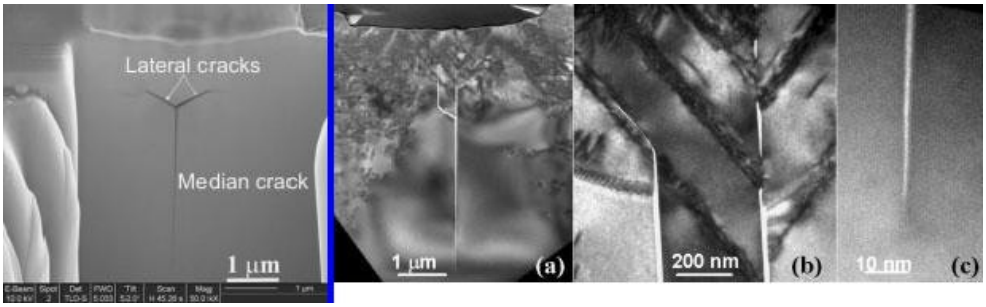

Figure 28: On the left: Median and lateral crack. The plastic deformation made with the diamond tip is seen in the top of the picture. On the right side of the blue bar: a) The median crack is propagating downwards and the lateral crack propagates in the lateral direction. b) A zoom of the starting point of the crack. The dark colored stripes are the (111) slip planes. c) A zoom in of the point of the median crack. The tip is atomically sharp and no other kinds of deformation are present.

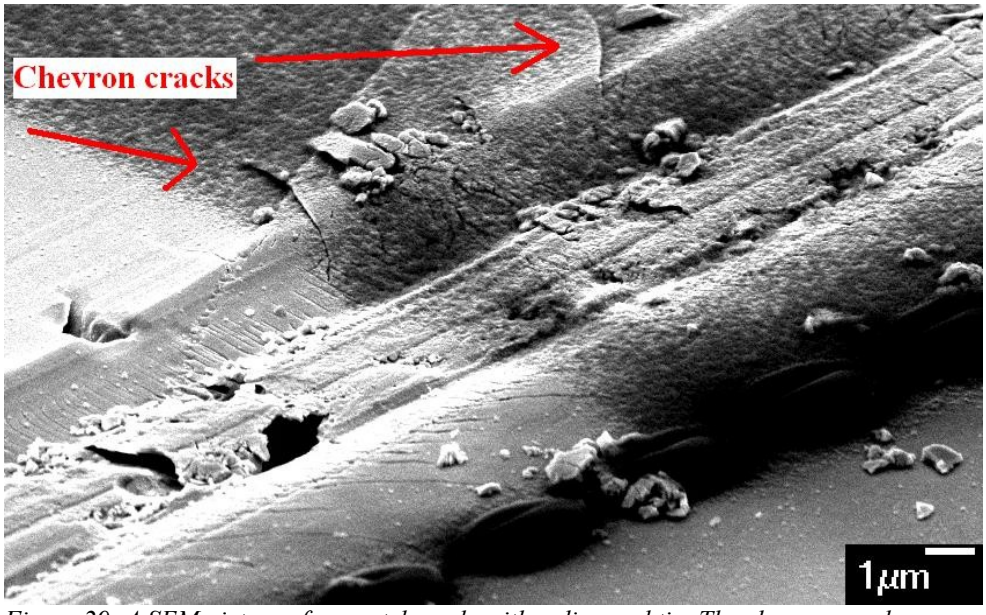

Figure 29: A SEM picture of a scratch made with a diamond tip. The chevron crack radiating out of the scratch are clearly viable.

Postscript

Cleaving Theory

During the writing of this thesis no relevant articles explaining the theory behind the scribing process could be found. The reason for this was due to searching with incorrect searching terms. It appears that there is theory about the process of scribing a wafer and subsequently cleaving it however this theory is relatively new, 2000 and later, and not easy to find. The search term leading to this theory was also the name of the physical process which enables the use of scribing to cleave wafers. This physical effect is called the median crack and will be explained after a short overview of the different phenomena's involved with scribing a wafer with a diamond tip.

Wafer deformation due to tip loading

The different stages involved with deformation of a wafer by a diamond tip which scratches over the wafer surface as function of the normal load with which the tip presses on the wafer surface is shown in figure 27. All values and characteristics mentioned will with reference to a GaAs wafer.

The first deformation visible is elastic deformation, it is reported to occur under a load of less then 4 mN **[1]**. In creasing the load to more then 4 mN will result in plastic deformation although there still is a considerable amount of plastic recovery. At a load of 10 mN the deformation results in a initial depth of 160 nm which after recovery is reduced to 50 nm relating to a elastic recovery of 110 nm**[1]**. In this lading range it is also possible the crystal will undergo phase transformations **[2]**. With the load increasing over 10 mN subsurface cracks are formed of which there are 2 different varieties. The median crack and lateral cracks of which the first is the reason cleaving a scribed wafer results in breaking of the wafer in one crystallographic plane over the entire length of the scratch.

The median and lateral crack

In figure 28we see a cross sectional view of a scratch made by Focused Ion beam Milling (FIB). As we can see deformation of the wafer surface with a diamond tip results in the formation of subsurface cracks. The median crack propagates into the wafer and is atomically sharp. At the point of the median crack there are no other kinds of deformation present. Cleaving of the wafer will result in the propagation of fracture at the position of the atomically sharp point of the median crack thereby resulting in a wafer cleaved over one single crystallographic plane. The depth of the median crack seems to correspond with the function know from Vicker indentations of brittle solids:

$$d \sim c \cdot F^{\frac{2}{3}}$$

where d is the depth of the median crack, c is a function of the geometry of the diamond tip used and scratching speed and F the force with which the scratch is made. The median crack depth is very consistent over the compete length of the scribe. The roughness of the cleaved facet is highly depended on the breaking characteristics of the wafer. This in turn is a function of the median crack depth. It is known that cleaving a wafer with a shallow median cracks results in catastrophic wafer cracking **[3]**. When continuously increasing the load to cleave a sample the load will buildup until a critical point at which the wafer will completely break though the full depth of the wafer. All the energy is immediately dissipated in the wafer and deformation of the cleaved facet will result.

A second type of crack is also formed which is called the lateral crack. This crack has no useful purposes in cleaving the wafer but might cause for some side effects influencing the scribe quality. The lateral crack is formed after the load is removed from the wafer e.g. when the diamond tip has moved on beyond the point of deformation **[6]**. Unlike the median crack The lateral crack size varies greatly over the length of the scribe.

The negative effects of the lateral crack will be discussed in the following section.

Chevron cracks and wafer chipping

When the load is increased beyond 10mN not only subsurface but also surface deformation starts to show apart from the plastic deformation of the wafer surface. These deformations are cracks radiation away from the scribe with a curved path. The cracks are called chevron cracks (see figure 29). The chevron cracks can have profound influence on the crack propagation of the wafer when cleaved. A chevron crack radiates away from plane where the median crack is formed. When the scribe is made such that it is not collinear with the preferred cleavage plane of the specific crystal a chevron crack might cause the cracking propagation the change into a more energetically favorable plane. This might for instance happen when trying to break a (111) grown wafer in squares **[4]**.

Chevron cracks can cause another important problem generally encountered when scribing a wafer. When a lateral crack penetrates all the way to the wafer surface and intersects with a chevron crack it will cause the wafer to become chipped it might also cause small particulates to be launched out of the wafer which then hit the surrounding wafer causing damage to the wafer top layer **[5]**.

Since the chevron cracks always radiate out from the scribe in the same manner the scribe direction can be deduced after wards.

This is only a short summary of the various effects coming into play when scribing a wafer. More condition have influence on the breaking quality and debris production during respectively cleaving and break which are not discussed i.e. the diamond tip geometry, loading geometry of the wafer during cleaving, wafer composition and more. Also in this overview the main focus is on the scribing of the wafer thereby missing the theory of the cleaving process up to a large extent. To have a more profound understanding of the physical processes involved with scribing and subsequently cleaving a wafer it is highly recommended to read the articles to which are referred in this overview.

References

[1] Wasmer, K., Ballif, C., Pouvreau, C., Schulz, D., Michler, J., 2008. Dicing of gallium–arsenide high performance laser diodes for industrial applications. Part I. Scratching operation. J. Mater. Process. Technol., 198, 114–121.

[2] Wasmer, K., Ballif, C., Gassilloud, R., Pouvreau, C., Rabe, R., Michler, J., Breguet, J.M., Solletti, J.M., Karimi, A., Schulz, D., 2005. Aspects of cleavage fracture of brittle semiconductors from the nanometre to the centimetre scale. Adv. Eng. Mater. 7, 309–317.

[3] K. Wasmer, C. Ballif, C. Pouvreau, D. Schulz, J. Michler., 2008. Dicing of gallium–arsenide high performance laser diodes for industrial applications. Part II. Cleavage operation, J. Mater. Process. Technol. 198, 105–113.

[4] A. Misra and I. Fininie., 1979. On the scribing and subsequent fracturing of silicon semiconductor wafers, J. Mater. Science 11, 2567-2574. figure 7

[5] A D Oliver1, T A Wallner, R Tandon, K Nieman, P L Bergstrom 2008. Diamond scribing and breaking of silicon for MEMS die separation, J. Micromech. Microeng. 18, 075026-075034

[6] B.R. Lawn, M.V. Swain., 1975. Microfracture beneath point indentations in brittle solids J. Mater. Science 10, 113-122.